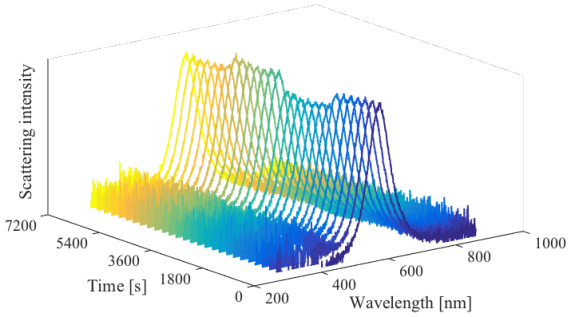
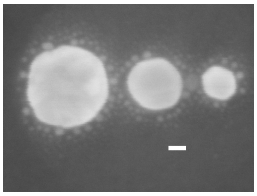
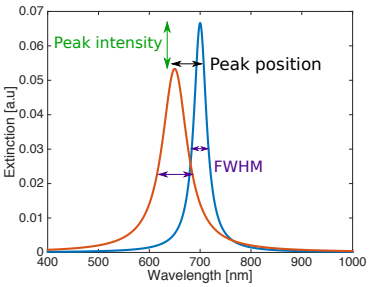
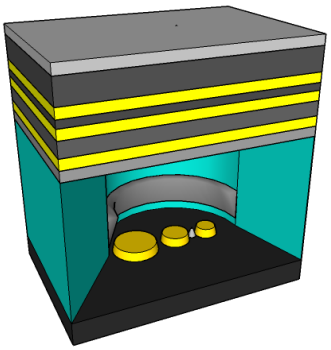
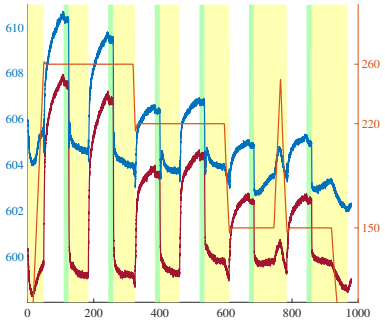
CHALMERS
UNIVERSITY OF TECHNOLOGY











Complex Plasmonic Nanostructures for Materials Science and Catalysis

Master's thesis in Applied Physics

David Albinsson

Department of Applied Physics
Chalmers University of Technology
Gothenburg, Sweden 2015

Master's thesis 2015

Complex Plasmonic Nanostructures for Materials Science and Catalysis

DAVID ALBINSSON



CHALMERS
UNIVERSITY OF TECHNOLOGY

Department of Applied Physics
Division of Chemical Physics
Chalmers University of Technology
Gothenburg, Sweden 2015

Complex Plasmonic Nanostructures for Materials Science and Catalysis

David Albinsson

© David Albinsson, 2015.

Supervisor: Svetlana Syrenova, Chemical Physics
Examiner: Christoph Langhammer, Chemical Physics

Master's Thesis 2015
Department of Applied Physics
Division of Chemical Physics
Chalmers University of Technology
SE-412 96 Gothenburg

Cover: Upper Left: Scattering spectra from Au-Cu structure when exposed to different gases.
Upper middle: SEM image of trimer consisting of Au disks
Upper right: Schematic showing changes of plasmonic peak properties due to changes in a LSPR active structure.
Lower left: Schematic image showing deposition of trimer structure using SHCL.
Lower right: Plasmonic peak position response of Au-Cu structures when exposed to varying gas compositions.
Typeset in LaTeX
Gothenburg, Sweden 2015

Complex Plasmonic Nanostructures for Materials Science and Catalysis
David Albinsson
Department of Applied Physics
Chalmers University of Technology

Abstract

Fabrication of arrays of identical nanoparticles in an efficient way using self-aligning systems is important to be able to scale up the production of nanoparticle based systems, for example for nanoplasmonics applications. In this thesis the possibility to use Shrinking Hole Colloidal Lithography (SHCL) as a method to fabricate complex nanoplasmonic structures using a wide set of materials has been explored. It is shown that SHCL can be used for fabricating complex structures with the ability to fine-tune details down to a size of a few nm. As case studies to demonstrate the functionalities of the obtained structures, the method has been used to measure the plasmonic response to hydride formation in sub-15 nm Pd nanoparticles, and the behaviour of Cu nanoparticles when exposed to different gas environments. The ability to use indirect plasmonic sensing as a probe for oxidation and reduction in Cu has been demonstrated both at the ensemble and single nanoparticle level.

Keywords: Plasmonics, nanostructures, nanoantenna, sensing, LSPR, copper, palladium, nanofabrication, SHCL, HCL.

Contents

1 Introduction **1**

2 Theoretical background **5**
2.1 Optical properties of metallic nanoparticles 5
2.1.1 Electrons in a small metallic particle 6
2.1.1.1 Electrons in a metal 6
2.1.1.2 Quasistatic regime 7
2.1.2 Deviations from the ideal theoretical system 8
2.1.3 Going even smaller 9
2.2 Plasmonic sensing 9
2.2.1 Direct sensing 9
2.2.2 Indirect sensing 10
2.2.3 Plasmonic antennas 11
2.2.3.1 Self-similar chains of nanoparticles 12
2.3 Hydride formation in metal nanoparticles 13
2.4 Oxidation and reduction of Cu 14

3 Fabrication of nanostructures **17**
3.1 Available methods 17
3.1.1 Top-down methods 17
3.1.2 Bottom-up methods 18
3.2 Hole-mask colloidal lithography 18
3.2.1 Spin coating 18
3.2.2 Plasma etching 19
3.2.3 Vacuum deposition 19
3.2.4 Fabrication steps of HCL 20
3.2.5 Shrinking-hole colloidal lithography 22
3.2.5.1 Cr funnel 22

4 Characterization methods **25**
4.1 Optical spectroscopy 25
4.1.1 Polarized light 26
4.2 Scanning electron microscopy 26
4.3 Hydrogen sensing 27
4.4 Oxidation and reduction experiment setup 27

4.5 Single particle spectroscopy 27

5 Fabricated structures **31**
5.1 Fabrication of plasmonic trimer 31
5.1.1 Evaluation of fabricated structures 31
5.1.1.1 Cr funnel method 31
5.2 Au-Cu structures for indirect sensing of oxidation and reduction of metal nanoparticles 34
5.3 Effects of annealing 36

6 Results **39**
6.1 Trimers for H_2 sensing 39
6.1.1 Optical spectrum 39
6.1.2 Hydride formation 39
6.2 Indirect sensing of oxidation and reduction of Cu nanoparticles 40
6.2.1 Plasmonic response using unpolarized light 41
6.2.1.1 O_2 response 41
6.2.1.2 H_2 response 43
6.2.2 Polarization dependence 43
6.2.2.1 Temperature ramps 44
6.2.2.2 Cycles 46
6.2.3 Effects of redox cycles on the structures 50
6.3 Single particle spectroscopy of Au-Cu Dimer 51
6.3.1 Au-Cu structure at different temperatures 52
6.3.2 Reference measurements on single Au disk 54

7 Conclusions **57**
7.1 Outlook 57

Bibliography **60**

1

Introduction

Ever since the roman empire, human made objects that somehow involve the optical properties of metallic nanoparticles have been something that amazed people. One of the first known objects where nanoparticles have been used to give it its characteristic optical properties is the Lycurgus Cup[1]. This cup has a glass tinted with gold and silver particles of the size of about a millionth of a centimeter which results in it having a different color depending on from which side it is illuminated.

Back then the craftsmen probably did not know that they were using the properties of particles of the size of 50 nm to give color to their beautiful objects but nonetheless, nanoparticles had a place in their lives. Inventions like the electron microscope has since made it possible for us to take a closer look at what the nano-world looks like, and as a result we can try to understand it. On the path of understanding the small parts of nature we can also try to build our own nano-sized objects with properties tailored to our needs. Understanding and using the world around us on the nano-scale will both enrich our knowledge about the world and can potentially help us to make it a better place. However it is also critical to understand and control the associated risks. Today nanoparticles can be found in almost all advanced materials related fields ranging from medicine to energy and electronics, and it is most certain that the understanding and usage of these materials will play a significant role in the future.

Even though our understanding of the nano-world has grown substantially, there are still applications of nanoparticles where we have yet to explain what is going on at the nano-scale. One such example of where nanoparticles are used widely and extensively is in catalysis. Catalysts often consist of networks of nanoparticles that act as reaction sites to increase reaction rates or steer reactions in a favorable direction. Solid catalyst are often made of metallic nanoparticles that enable large specific surface areas, as well as an appreciable amount of highly active sites for reactions to occur on. Even though catalysts have been improved there are still uncertainties to how they work and exactly what happens with the atoms partaking in the reactions. Catalytic processes are often complicated with many intermediate steps before reaching the final product. Therefore methods to study catalysis both have to be able to detect changes on a (close to) molecular scale and at the same time have a good temporal resolution. Catalytic particles and the reactions occurring on their surfaces are also very sensitive to the surrounding conditions such as temperature, pressure and support material. Because of this it is important to try to mimic real conditions as much as possible when researching catalysts. Ideally one would like to have what is called an *in-situ* measurement device that could measure catalytic activity in a *real* reactor where

the conditions are the same as when they will be used in the targeted industrial or environmental cleanup process. Thus, to further understand catalysts, methods to investigate how specific material and structural properties of individual nanoparticles effect the resulting catalytic performance have to be developed. Many methods used today are capable of studying large samples of nanoparticles and their performance, but such studies only give information of an average structure. It is of interest to know how individual nanoparticles perform depending on their size and shape. To do this, methods enabling single particle studies have to be developed. This is a challenge, because as the size of the studied system decreases, so does the observable signal.

During the past two decades the interest in what is known as surface plasmons has grown rapidly. The electron oscillations induced in metallic nanoparticles when exposed to light occur due to a phenomenon known as localized surface plasmon resonance (LSPR). The resonance characteristics of LSPR are sensitive to the surroundings of the nanoparticle and therefore show great promise as sensors in a number of fields such as biosensing and chemical sensing[2–5].
To further utilize the effects of LSPR certain structures of plasmonically active nanoparticles have shown to result in strongly enhanced electromagnetic fields in very small volumes. Structures that enhance the field in this way are known as plasmonic antennas and they have shown great promise as sensors[2,4,5], but also for steering light for other purposes such as amplifying photovoltaic devices[6,7].
Because LSPR-active nanoparticles interact so intensively with light it is possible to see scattered light coming from a single particle when viewing it in a dark-field microscope. This impressive feature opens the possibility to make sensors based on single nanoparticles where the scattering spectrum of a single plasmonic structure is measured while changing the surrounding conditions[8,9].
With some imagination one could then think of placing several single particle sensors on one chip, making it possible to create universal sensors for many compounds on a device no larger than a fingernail.

The goal of this thesis

In this thesis the possibility to use localized surface plasmon resonance (LSPR) as a tool for studying both ensembles and single particles of catalytically active particles has been investigated. Much of this thesis work was about exploring a new way to fabricate complex plasmonic nanostructures for application in sensing of the hydrogenation or oxidation state of reactive nanoparticles *in-situ* and in real time. The goal was to develop a reproducible way to fabricate complex structures consisting of several different materials with different specific function, and to be able to finely adjust the sizes and positions of the deposited structures. The first structures fabricated where trimers of Au disks with decreasing size with a small Pd nanoparticle placed in a spot with a highly enhanced EM-field. The specific geometry of the gold trimer, known as a self-similar chain, was chosen based on the theoretical work showing that it has a particularly effective enhancement of the EM-field[10]. The plasmonic as well as sensing properties of the fabricated structures where then assessed.

As a second part of the thesis, structures consisting of a single Au disk acting as an antenna with a reactive Cu particle placed next to it was fabricated. The plasmonic response of the system due to oxidation and reduction of the Cu nanoparticle was measured for both ensembles of structures and single particles in an attempt to derive the Cu oxidation state *in-situ*.

2

Theoretical background

This chapter has the ambition to give a background of the theoretical concepts used to explain the experiments performed in this thesis. The largest part of the background tries to explain LSPR in a simple manner. For a much more complete description of the phenomena I would recommend reading one of the many books on the subject[11,12].

2.1 Optical properties of metallic nanoparticles

Optical properties of metals are at a bulk scale governed by the band structure and give rise to the "metallic" look they have. However, metallic particles with a size smaller than the wavelength of an incident electromagnetic wave interact with light differently. Because the particle is small, the incident lightwave is able to penetrate the whole particle and make all free electrons in the particle move in an organized fashion. Due to the wave-nature of light the resulting motion of the electrons will be an oscillation. Figure 2.1 shows the behavior of the electron cloud at two different times of an applied lightwave. Because of the particle's small size, all electrons will, in a first approximation, feel the same applied field at any given time, giving rise to a collective and coherent motion of the electrons. The oscillation of electrons confined to a nanoparticle is known as a localized surface plasmon (LSP). If the frequency of the incoming electromagnetic wave matches the resonance frequency of the electrons in a nanoparticle the interaction with light will be maximized resulting in Localized surface plasmon resonance (LSPR).

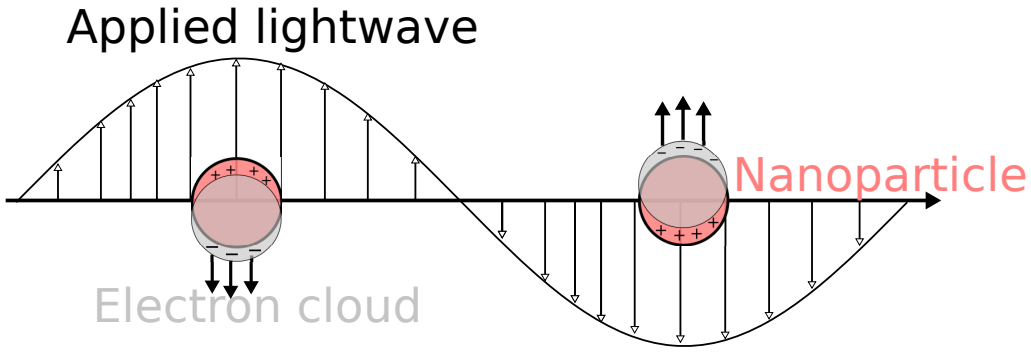


Figure 2.1: Plasmonic nanoparticle affected by a incident electromagnetic wave. The two structures illustrate the same particle at different times.

2.1.1 Electrons in a small metallic particle

To explain the physics behind LSPR a simplified model system consisting of a perfect metallic sphere will be considered.

2.1.1.1 *Electrons in a metal*

A simple model for explaining the behavior of electrons in a metal under the influence of an external electric field comes from the Lorentz-model. In this model the motion of the electrons is explained by the classical equation of motion of a driven harmonic oscillator:

$$m_e \frac{\partial^2 \mathbf{r}}{\partial t^2} + m_e \Gamma \frac{\partial \mathbf{r}}{\partial t} + K\mathbf{r} = -e\mathbf{E} \tag{2.1}$$

where $\mathbf{E}$ is the applied electric field, m_e is the electron mass and Γ is a damping factor, K is the spring constant and $-e$ is the electron charge. Solving this yields:

$$\mathbf{r} = -\frac{e/m_e}{\omega_0^2 - \omega^2 - i\Gamma\omega}\mathbf{E} \tag{2.2}$$

with the electric dipole moment:

$$\mathbf{p} = -e\mathbf{r} = \frac{e^2/m_e}{\omega_0^2 - \omega^2 - i\Gamma\omega}\mathbf{E} \tag{2.3}$$

where

$$\omega_0 = \sqrt{K/m_e} \tag{2.4}$$

To expand this equation from a single electron to many electrons an electron density N is introduced. The dipole moment per unit volume can then be expressed in terms of a dielectric function ($\varepsilon(\omega)$) as:

$$\mathbf{P} = N\mathbf{p} = \varepsilon_0(\varepsilon(\omega) - 1)\mathbf{E} \tag{2.5}$$

where ε_0 is the permittivity of vacuum and

$$\varepsilon(\omega) = 1 + \frac{\omega_p^2}{\omega_0^2 - \omega^2 - i\Gamma\omega} \tag{2.6}$$

is the dielectric function of the material[11] and ω_p is the plasma frequency of the electrons expressed as:

$$\omega_p = \sqrt{\frac{Ne^2}{m_e\varepsilon_0}} \tag{2.7}$$

According to the Drude-model, electrons can be treated as free electrons traveling through a sea of comparably stationary ions. This theory can be considered valid in a metal because

electrons close to the Fermi level have many electronic states with a slightly higher energy to occupy and therefore they feel no significant potential that forces them to stay in place. This makes it possible to assume that $K = 0$ in eq. (2.4), which simplifies eq. (2.6) to the form:

$$\varepsilon(\omega) = 1 - \frac{\omega_p^2}{\omega^2 + i\Gamma\omega} \tag{2.8}$$

2.1.1.2 *Quasistatic regime*

The next assumption made is that the size of the metallic particle is noticeably smaller than the wavelength of light. To interpret the effect this assumption has on the system, an example is presented in fig. 2.1. In this image the particle is much smaller than the wavelength of the incident light. Because of this, within reasonable approximation, the effective applied field on the particles can be seen as the same for all electrons. Effectively, all electrons in the particle will move in the same direction, making the particle act as a dipole. This assumption removes the variation of the electromagnetic field in space over a single particle and is called the quasistatic approximation.

As a result of this the sphere can be seen as a point electric dipole. The induced dipole moment from an applied plane wave can be expressed as[11,12]:

$$\mathbf{P}(\omega) = \varepsilon_d \alpha(\omega) \mathbf{E}_0 e^{-i\omega t} \tag{2.9}$$

where ε_d is the dielectric constant of the surrounding medium and $E_0 e^{-i\omega t}$ is the incident electric field and α is the polarizability of the material. Presuming our material is a metallic sphere with dielectric function ε_m the polarizability is given by[11,12]:

$$\alpha(\omega) = 4\pi\varepsilon_0 r^3 \frac{\varepsilon_m(\omega) - \varepsilon_d}{\varepsilon_m(\omega) + 2\varepsilon_d} \tag{2.10}$$

where r is the radius of the sphere. Worth to note is that α depends on both the properties of the metallic nanoparticle (ε_m and r) and the surroundings (ε_d).
Depending on the properties of incident light and the material properties of the sphere the resulting light-particle interactions will differ. The efficiency of the different interaction processes are expressed as cross-sections and they can be expressed for extinction, scattering and absorption, respectively[11]:

$$C_{absorption} = kIm(\alpha) \tag{2.11}$$

$$C_{scattering} = \frac{k^4}{6\pi} abs(\alpha)^2 \tag{2.12}$$

$$C_{extinction} = C_{absorption} + C_{scattering} \tag{2.13}$$

where $k = 2\pi/\lambda$ is the wavenumber of incident light. This shows that maximizing the polarizability (2.10) will maximize both the scattering and absorption efficiency of a particle.

The size-dependence of the particle for absorption is scaled as the volume of the particle (r^3) while for scattering it scales as volume^2(r^6). This implies that for very small particles absorption will dominate and for larger particles scattering will be the dominating process. From eq. (2.10) it can be seen that the polarizability is maximized when:

$$\varepsilon_m(\omega) + 2\varepsilon_d \to 0 \tag{2.14}$$

which leads to diverging polarizability when:

$$\varepsilon_m(\omega) = -2\varepsilon_d \tag{2.15}$$

The damping factor Γ is related to non-radiative processes in the system that can relax an excitation. The most commonly regarded non-radiative process that affects the damping factor is absorption where an electron-hole pair is excited in the material resulting in the dissipation of the energy often as heat via electron-phonon coupling. Many processes taking place in the real systems will be affected by the damping factor but for simplicity of the model it will be seen as negligible.
By combining (2.15) and equation (2.8) and assuming a negligible damping Γ the resulting LSPR frequency is:

$$\omega_{LSPR} = \frac{\omega_P}{\sqrt{1 + 2\varepsilon_d}} \tag{2.16}$$

This derivation of the resonance frequency of a spherical metallic nanoparticle was done to give a sense of the basic physics governing LSPR. As a system deviates from the ideal model system the assumptions made will no longer be valid and the resulting resonance frequency and the corresponding interactions with light will be different. To model more complex systems more detailed mathematical models have to be used to give a better explanation of the real physics. Mathematical models of this kind are often based on methods such as finite differential time domain (FDTD) and discrete dipole approximation (DDA) that makes it possible to numerically handle more complex structures[13].

2.1.2 Deviations from the ideal theoretical system

As for all real-world applications the structures created during this thesis are not perfect. Even small changes of the size and shape of a nanoparticle will effect the resulting interaction with light. The effects of geometrical deviations from the ideal case have been studied both experimentally and theoretically. Surface roughness has shown to change the optical properties of plasmonic structures[14] and it is therefore hard to directly predict what the optical properties of a certain plasmonic structure will look like. To be able to study how small structural properties effect the properties of a particle it is necessary to have methods that allow studying structures one at the time. This can be a complicated task because nano-sized objects are hard to confine and the signal to noise ratio of measurements taking place on single particles is often very low. Because LSPR active particles strongly interact

with light resulting in scattered light it is possible to measure changes in single particle by studying the scattering spectrum[4,8,9,15]. The knowledge gained from studying single particles where specific geometrical anomalies can be taken into account makes it possible to improve the theoretical models used to predict the optical properties of these structures.

2.1.3 Going even smaller

Commonly the approximations made for a theoretical description of plasmonic systems rely on a model based on classical electrodynamics. Solving Maxwells equations for shape, material and surrounding gives information of the electromagnetic field that arises in and near the structures. Classical electrodynamics is, however, of limited use when the dimensions of the system decrease bellow a few nm. The limit between when a group of metal atoms has to be considered a large molecule instead of a small piece of bulk metals has to be kept in mind as our methods of fabrication enable us to go smaller every year. Recent studies have investigated the limit where quantum mechanics has to be considered to see the whole picture and atomistic models have shown plasmonic coupling between the electrons of single atoms in small metallic clusters[16,17]. Including quantum mechanical effects in the theoretical models for describing plasmonic systems makes the latter even more complex. But to be able to model smaller systems and continue the decrease in size this is something that should be kept in mind.

2.2 Plasmonic sensing

As has been shown above the plasmonic properties of a metal nanoparticle depend on the dielectric properties of the LSPR active material, the size of the particle and the particle's surroundings. A change in one of those properties is expected to induce a measurable change in the optical spectrum. By measuring absorption and/or scattering from LSPR active structures small changes in or around the particle can therefore be detected. The LSPR peak is characterized with the standard peak parameters: peak position, maximum peak intensity and full width at half maximum (FWHM). In fig. 2.3a measurable changes in the peak characteristics are indicated by arrows.

2.2.1 Direct sensing

Effects of changes in different plasmonic particles have been demonstrated both theoretically and experimentally[5]. The method of actively monitoring plasmonic materials by looking at their extinction or scattering spectrum has shown to be a powerful method to get real time information about reactions taking place. The method of directly sensing changes in a LSPR active material by monitoring changes in the structure itself is know as direct plasmonic sensing. A limitation to direct sensing is that the material of interest has to be a good localized surface plasmon resonator itself. The most commonly used materials with known good plasmonic peaks are silver (Ag) and gold (Au), but the other metallic

and semiconducting materials can also be used[2]. The problem with some metals is that they themselves undergo chemical reactions and transform into something non-metallic. This transition could result in the studied material loosing the plasmonic peak. It is also required that the measured particle is large enough to acquire a measurable change in their signal.

Extra info about Cu When Cu nanoparticles form an oxide shell it strongly damps the plasmonic resonance strength[18]. Cu in its metal state has free electrons and has a clearly visible plasmonic peak in the visible range. The oxides it forms on the other hand are semiconductors and they do not have the same type of strong plasmonic peak.

2.2.2 Indirect sensing

An alternative sensing method is to use a chemically inert material with a strong plasmonic resonance as an antenna to detect changes in a second material placed nearby[5].
For a simple structure like a disk or sphere, the sensing volume is located in the near field around the plasmonic particle. The spatial extension of this near field from the plasmonic particle surface depends on the structure used but for a simple sphere it has been shown to be of the size of a few to tens of nanometers[5,19]. In fig. 2.2 a plasmonic disk exited by polarized light indicated by the arrows is presented with the sensing volume indicated in color. In fig. 2.3 a schematic image of changes in a small particle close to a larger LSPR-active antenna is presented. As seen in the previous section, the resonance frequency of a plasmonic nanoparticle depends on the dielectric function of its surrounding. Because of this, a change of the dielectric constant of a material close to a LSPR-resonator will change the resonance frequency and can therefore be measured.
This kind of sensing has been shown to work for different applications such as measuring changes in small Pd particles placed on top of a larger Au disk[20]. Pd reacts with hydrogen forming a hydride which changes both the size of the Pd and the dielectric function of the material. These changes are then picked up by the inert Au disk resulting in a change in the LSPR peak of the material.

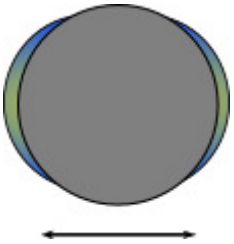
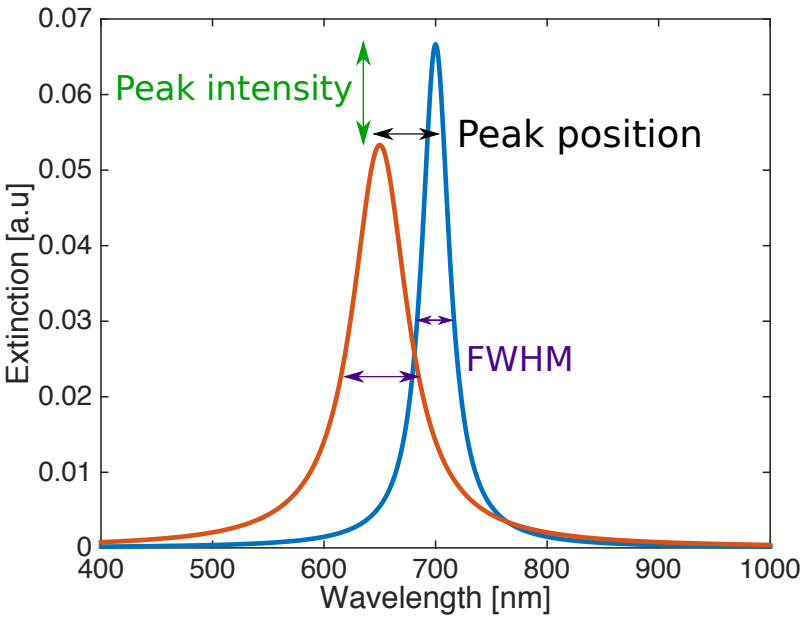


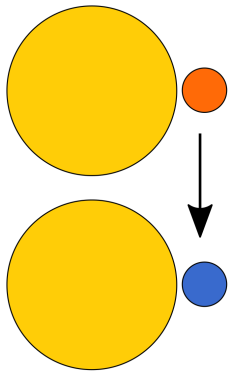
Figure 2.2: Plasmonic disk with sensing volume.

If the material placed in vicinity to the antenna is also a plasmonically active material, coupling will occur among the two. A simple way to think about it is to see the two particles as classical oscillators connected to each other by a spring. This coupling will give rise to new possible modes which can be both enhancing and destructive. Changing the dielectric

properties (can be seen as changing the mass or spring constant of a classical oscillator) of one of them will therefore affect their resulting optical spectrum. This can be utilized for indirect sensing of, for example, oxidation in a Cu disk close to a larger Au disk acting as an antenna.



(a) Changes in peak properties



(b) Indirect sensor for detection of reactions taking place in the small structure to the right of a larger Au disk acting as an antenna.

Figure 2.3: Changes in LSPR peaks that are monitored when changing properties in or around the plasmonic antenna showed as a large yellow circle.

2.2.3 Plasmonic antennas

The dipoles formed when the free electrons are moved in one direction as illustrated in fig. 2.1 will in turn give rise to an induced electric field. This induced field will be localized close to the particle and the total field in and around the particle will be the sum of the applied field and the induced field. Different antenna geometries have been demonstrated as efficient antennas such as trimers and triangles with sharp corners[4,7,21–23].

By varying the shape of particles the electromagnetic field can be steered to certain spots where the enhancement of the field becomes particularly high. This, in turn, should maximize the sensitivity of the LSPR to the dielectric changes occurring in this particular spot.

The volume close to a plasmonic antenna with the highest enhancement of the EM-field is known as a hot-spot. Because of asymmetries in structures with other shapes than single spheres or disks the polarization of incident light will affect the plasmonic response. This is because the coupling between the plasmonic oscillations of several nanoparticles depends on the direction they oscillate. For a dimer structure consisting of two identical particles the polarization of light can be in line with the two particles, resulting in coupling between the two oscillations. If the light instead is polarized perpendicular to the axis connecting the two particles the plasmonic modes will behave much more as two individual spheres.

In fig. 2.4 the polarization dependence of the enhanced field around a dimer structure is presented. Because coupling between particles close to each other will create new possible oscillation modes, the resulting LSPR frequency will be different than the single particle case. In case of two spherical nanostructures, they can oscillate with the same phase resulting in dipoles pointing in the same direction that in turn has shown to enhance the induced field between the two particles[24]. If the two spheres instead oscillate in opposite phase the two dipoles cancel out resulting in a diminished field between them.
By fabricating specific structures the coupling can be tailored to have a maximized enhancement in a very spatially constricted volume. A dimer of two identical spherical nanoparticles placed at a short distance from each other has shown to efficiently enhance electromagnetic field between them[25]. In the work by Syrenova et.al.[25] dimers of two identical Au disks were used as antennas to detect a signal from hydrogenation of a small Pd particle placed in the dimer hotspot between the two disks. The enhancement resulting from a dimer antenna made it possible to do single particle measurement of hydrogenation of Pd particles down to a size of 14 nm.
More complex geometrical structures have also been suggested in theoretical studies to have even higher enhancement and more spatially confined hotspots[4,7,10,22].

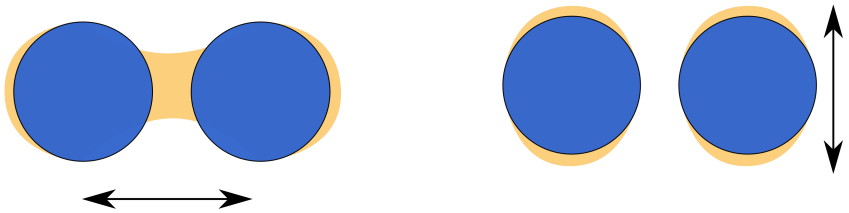


Figure 2.4: Enhanced field around plasmonic nanoparticles depending on the polarization of incident light indicated by arrows. To the left the enhanced field is strongest between the two particles due to coupling between the oscillating electrons of the two particles. To the right the electrons do not couple in the same way and the enhanced fields are instead more like the single particle case.

2.2.3.1 *Self-similar chains of nanoparticles*

One of the configurations of nanoparticles that has shown interesting results in theoretical studies is the self-similar chain of plasmonic nanoparticles[10,22]. This structure uses a chain of similarly shaped nanoparticles with decreasing size placed in a line. This creates a cascade effect where the second particle feels the first particle's enhanced field as an addition to the applied field, and as the chain grows, the fields in the gaps between the particles grow rapidly. For a self-similar chain the size should decrease as:

$$D_n = \kappa D_{n-1} \tag{2.17}$$

where D is the diameter of the particle and κ is a constant <1. This configuration has shown to have the "hottest-spot" between the smallest and the second smallest particle[10]. This spot also shows the most spatially confined enhancement which enables very precise enhancement with great amplification.

An example of a self similar chain of round structures is presented in fig. 2.5.

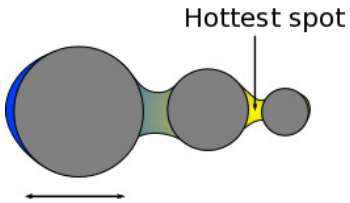


Figure 2.5: Self similar antenna

2.3 Hydride formation in metal nanoparticles

Hydrogenation of Pd and the corresponding plasmonic response of systems consisting of Pd paired with Au structures is well studied[3,9,20,26]. Pd structures placed close to a larger Au particle acting as a plasmonic antenna has shown to be a good sensor for detection of the presence of hydrogen and the expected plasmonic changes corresponding to introduction of hydrogen are known. Therefore hydrogen sensors based on Au and Pd were used as a model system in this thesis to test if the fabricated structures worked as expected.

Hydride formation in metals such as Pd is a well studied phenomenon. From an energy related perspective the ability to hydrogenate and dehydrogenate metal nanoparticles is of interest for applications in hydrogen storage[5]. To be able to use hydrogen as a future fuel the ability to detect and measure the hydrogen present is also of great interest. Cheap, reliable and simple sensors and detectors have to be developed to be able to introduce hydrogen fuel to the market at a large scale. The hydrogen uptake and release in metal nanoparticles results in both a change in the structure of the metal and a change in its dielectric properties, and is in turn measurable by plasmonic sensing[27]. A well studied material for hydrogen storage is Pd. The plasmonic behavior of Pd nanoparticles has been investigated the past decade and it is therefore a good model system to use for detection of hydrogen. Unfortunately Pd nanoparticles have a very wide plasmonic peak in the UV-vis-NIR region due to inter-band transitions[26]. Direct measurements of the peak properties (position, intensity, FWHM) is therefore difficult because small changes of a very wide peak are hard to detect.
Changes of geometry and the dielectric properties of the material can be detected using indirect plasmonic sensing[4,5]. By placing the particle of interest close to a good plasmonic resonator, acting as an antenna, the changes in Pd can be indirectly measured by measuring changes in the plasmonic response of the antenna[27]. Previous work has shown that it is possible to build indirect plasmonic nanoantennas using shapes with sharp edges, such as triangles and rectangles[4,15] or dimers consisting of two symmetrical disks with a Pd placed in the gap between them[23]. By placing Pd in a spot with a greatly enhanced EM-field the limit of what could be detected could potentially be pushed to a smaller size. A structure that has potential as a good plasmonic nanoantenna is the self similar structure illustrated in fig. 2.5.

2.4 Oxidation and reduction of Cu

Cu is a metal used as a catalyst in many reactions, such as methanol synthesis[28,29] and the water-gas shift reactions[30], and could play an important role in synthesizing fuels in an energy efficient way. Catalytic materials often consist of nanosized particles that interact with the reacting components in a way that enables new reaction paths. To be able to fully understand the processes on an atomic level methods to study the exact chemical state of a catalyst in real time are needed because the catalytic reactivity and selectivity of an oxidized catalyst might be very different from a reduced (metallic) one. Methods that can do this today are usually complicated, expensive and require significant amounts of sample material. Methods that can be used to monitor nanoparticles in real time are for example: *in-situ* Scanning electron microscopy (SEM), Extended X-ray absorption fine structure (EXAFS), X-ray absorption spectroscopy (XAS). Unfortunately none of these methods are simple, portable or cheap. Plasmonic sensing has the potential of being a good in-situ detector of the changes taking place when reactions occur on or in metallic nanoparticles. This technique only requires a light-source and a corresponding detector to be able to monitor changes in real time and can therefore be made both small and relatively cheap.
To be able to monitor the state of Cu during a catalytic reaction we first have to know how the optical response of a plasmonic system containing Cu nanoparticles depends on the state of Cu. This knowledge could possibly be gained by studying the optical response of systems under conditions when Cu is known to undergo certain reactions. When pure Cu is placed in an oxygen containing environment it will oxidize and form an oxide. Depending on the conditions of the oxidation the resulting oxide state can vary[31]. At temperatures below 200°C it has been shown that Cu nanoparticles of about 20 nm form mostly the oxide Cu_2O when exposed to oxygen. As the temperature is increased Cu will be further oxidized resulting in the formation of CuO.

When Cu transforms from a metal to a semiconductor the electronic properties of the material undergo dramatic changes. By studying this process using direct plasmonic sensing the change of the optical spectra is large. This is because metallic Cu nanoparticles have a clear plasmonic peak but the oxides do not have free electrons that can create a LSP. The result of monitoring the LSPR-peak of Cu nanoparticles during oxidation is that a clear peak is visible at the start but as the particles react with oxygen the peak disappears[18]. Due to the large change in the optical properties of Cu during oxidation it can be hard to follow the oxidation process by monitoring a peak. The Cu particles also have to be large so that their interaction with light is measurable. As described in eqs. (2.10) to (2.13) the efficiency of a particle's interaction is strongly size dependent and therefore the intensity of interaction quickly diminishes when the size is reduced.
To be able to study smaller particles that themselves do not interact with light strongly enough to have a measurable signal indirect sensing could be used. In this thesis a small Cu particle placed close to a larger Au disk acting as an antenna is proposed to work as a detector of changes in the Cu nanoparticle. The reason for this is proposed to be due to changes in the dielectric function of Cu when oxidizing that give rise to measurable

changes of the optical spectra of the system. By comparing the optical response of a system consisting of Au-Cu pairs with previous data found for oxidation of Cu using other methods[31] the goal is to evaluate the possibility to use indirect plasmonic sensing as a technique for *in-situ* monitoring of Cu nanoparticles.

3

Fabrication of nanostructures

In 1959 Richard Feynman held a famous speech at Caltech with the title *There is plenty of room at the bottom*. He envisioned the whole Encyclopedia Britannica written on the tip of a needle and discussed the possibilities and limitations of fabricating things on scale that was unthinkable at the time. The speech can be seen as the start of a new field of technology known today as nanotechnology. Every year our ability to fabricate smaller and smaller structures in a controlled way is improved. This is probably most noticeable in everyday life in the electronics industry where the performance of small computers is improved every year. The reason behind this is that scientists come up with new and improved methods to fabricate smaller structures with the same, or better, performance as larger ones. In the electronics industry the size of a single transistor is a measure of how small things can be made. From the year 2000 to today the size of transistors has shrunk from 130 nm to 15 nm. In the scientific field many different methods for fabricating nano-sized objects are developed to make it both cheap and possible with simple equipment.

3.1 Available methods

The number of methods used for nanofabrication is constantly growing and each method is individually improved all the time. To distinguish between the main approaches to nanofabrication two groups are commonly referred to. They are known as *top-down* methods, where external tools are used to build small structures, and *bottom-up* methods, where one relies on small building blocks that self assemble and form desired structures.

3.1.1 Top-down methods

In this group there are several different methods that also can be divided into subgroups. One of those are so called pattern writing techniques. In these methods structures are typically written by focusing beams of particles (typically electrons or ions) onto small areas, which results in structuring of bulk material. Widely used methods of these kind of focused beam writing are electron beam lithography (EBL) and focused ion beam lithography (FIB) that have the capability of fabricating structural details down to a size of 5 nm. Another method of *top-down* fabrication is to use a nanosized tip to mechanically move structures to desired

places on a surface. These methods can be based on Scanning tunneling microscope- (STM-) or atomic force microscope- (AFM) like devices and have shown to be able to modify single atoms. The downside of the methods mentioned is that they require advanced equipment and they are only capable of fabricating one structure at a time, which makes them time consuming.

3.1.2 Bottom-up methods

Bottom-up approaches, on the contrary, are inspired by how nature builds complex structures. By mixing the right components and letting the system organize itself, complex patterns of identical structures can be made. This significantly reduces the need of advanced expensive machines and also makes it possible to modify structures on a molecular scale and therefore has a very small lower size limit.
Nanofabrication of the structures used in this thesis has been done using colloidal self-assembly. This refers to a process where a colloidal dispersion of nanoparticles is used to create a pattern due to interaction between the colloidal nanoparticles and the surroundings. By fabricating surrounding structures so they have a specific affinity for the colloidal particles the places where particles are placed can be controlled.
The following chapter is dedicated to explaining in detail how structures were fabricated using a technique named Hole-mask colloidal lithography (HCL)[32].

3.2 Hole-mask colloidal lithography

HCL is a *bottom-up* method that utilizes colloidal nanoparticles that self-assemble to create an evaporation mask. The mask is then used as a guide for deposition of nanoparticles. The HCL process can be divided into steps that will be explained in more detail in the following section. The steps are:

1. Spin coating
2. Plasma etching
3. Vacuum deposition

3.2.1 Spin coating

Spin coating is a technique used to create uniform films of materials on a substrate. As the name suggests it utilizes a spinning substrate to create a coating of a material on it. To perform spin coating a few drops of a viscous material are deposited on a substrate that needs to be covered. The substrate is then spun at high speed so the droplet is evenly distributed over the surface. The properties of the coating can be controlled by varying many factors. The main factors that affect the coating are: properties of the coating fluid (material, viscosity, evaporation rate), substrate (surface structure) and rotation (speed,

acceleration, time). All these factors have to be optimized to reach the required properties of the film.

3.2.2 Plasma etching

Plasma etching is a technique used to remove (etch) certain parts of the sample. The etching is made by a plasma which is a state of matter where the particles are locally ionized. This means that in a plasma there will be free radicals such as ions and electrons.
The device used for plasma etching in this thesis was the commercially available Plasma-Therm BatchTop. The main components of the plasma etch system are the anode, cathode and the plasma generator. In the system used in this thesis the plasma was generated by an electric field strong enough to strip the electrons from the reactive species (gas). When stripped from their molecules, the electrons, with their high mobility, quickly travel towards the anode. The positively charged ions left in the chamber then feel the negative charge from the cathode and start traveling towards it with high velocity. The radicals in the plasma are highly reactive and will therefore chemically react with the compounds on the cathode surface. In the end the plasma etching will etch both due to physical ion bombardment and due to the chemical reactions with the surface.
For this thesis an oxygen plasma was used to etch away parts of polymer thin films.

3.2.3 Vacuum deposition

Vacuum deposition is a technique that is used to deposit thin films of materials through physical vapor deposition (PVD). By evaporating a material in a vacuum chamber and allowing the evaporated molecules to travel to the substrate a thin film can be built. The vacuum is needed to be able to limit the number of collisions the molecules undergo on their way from the evaporation source to the substrate where they are deposited. Typically a pressure below 10^{-4} Torr is enough to eliminate collisions in an average sized evaporation chamber[33]. When collisions are not an issue the evaporated atoms can be considered to travel in straight lines from the source to the target where they are deposited. This makes it possible to treat the evaporation path as a parallel stream of material and by tilting the sample different structural parameters can be built. By controlling the evaporation rate and the time the substrate is exposed to the deposition, the thickness of the film can be controlled to the level of Ångstroms[33].
To heat the source material to the point of evaporation different methods can be used. Most common are resistive heating and electron beam heating. Depending on the material and the required precision different methods are best suited. For my work all evaporators used sources heated by an electron beam.
The evaporations took place in two different systems. Both were customized systems manufactured by LESKER. One was used for simple evaporations where control of tilt and rotation was not needed, this system was mostly used for depositing the mask in HCL. The second system had the possibility to tilt and rotate the substrate which was used to deposit nanodisks on the substrate through the hole mask and to shrink the hole in the mask.

3.2.4 Fabrication steps of HCL

In this method charged polystyrene (PS) nanoparticles are used to create an evaporation mask. The fabrication steps involved in using HCL to fabricate nanostructures are listed bellow. In fig. 3.1 the steps are illustrated to give a more clear picture of what happens on the small scale.

1 Substrate cleaning Substrate is cleaned with acetone, isopropyl alcohol (IPA) and methanol, each solvent followed by immersing the beaker in an ultrasonic cleaning machine for 3 minutes.

2 PMMA cover Poly(methylmethacrylate) is spincoated on the substrate. The aim is a PMMA layer of 280 nm and for that the spinner is set to a speed of 2000 rpm for 1 minute. The substrates are then placed on a hotplate at 170°C for 10 minutes to evaporate any remaining solvent.

3 Plasma etching A short etch by oxygen plasma is performed on the PMMA. This is to reduce the hydrophobicity of the substrate.

4 PDDA Poly(diallyldimethylammonium) (PDDA) in water solution is placed on the surface for 40 seconds followed by rinsing in water. This is done to create a thin positively charged layer on top of the PMMA. See fig. 3.1a.

5 PS particles A dispersion of polystyrene (PS) particles in water is placed on the surface for 3 minutes followed by 20 seconds rinsing in water, 40 seconds in hot (almost 100°C) water and another 20 seconds in cold water. The concentration of the PS solution was varied to be able to control the surface coverage of the final structures. The PS particles have a negative surface charge and therefore attach to the positively charged PDDA surface and at the same time repel each other, which results in a coverage with a typical nearest neighbor distance but without long range order. The size and concentration of PS particles determine the size of the holes in the mask and the surface coverage. See fig. 3.1b.

6 Mask evaporation A thin film (around 20nm) of a material of choice (Cr and Au used in this thesis) is evaporated on the surface covered with PS. See fig. 3.1c.

7 Tape stripping Tape is placed on top of the covered surface. When removed, the tape will take the PS particles with it leaving a mask with holes and the underlying PMMA exposed. See figs. 3.1d and 3.1e.

8 Plasma etching Plasma etching using oxygen is performed on the substrate. The metallic mask is resistive to oxygen plasma and the etching is performed through the holes on the underlying PMMA. By adjusting time of the etching the amount of removed PMMA can be controlled. A longer time results in a larger undercut, meaning that the PMMA is etched parallel to the substrate surface to create a hole that has a larger diameter than the hole in the mask. See 3.1f.

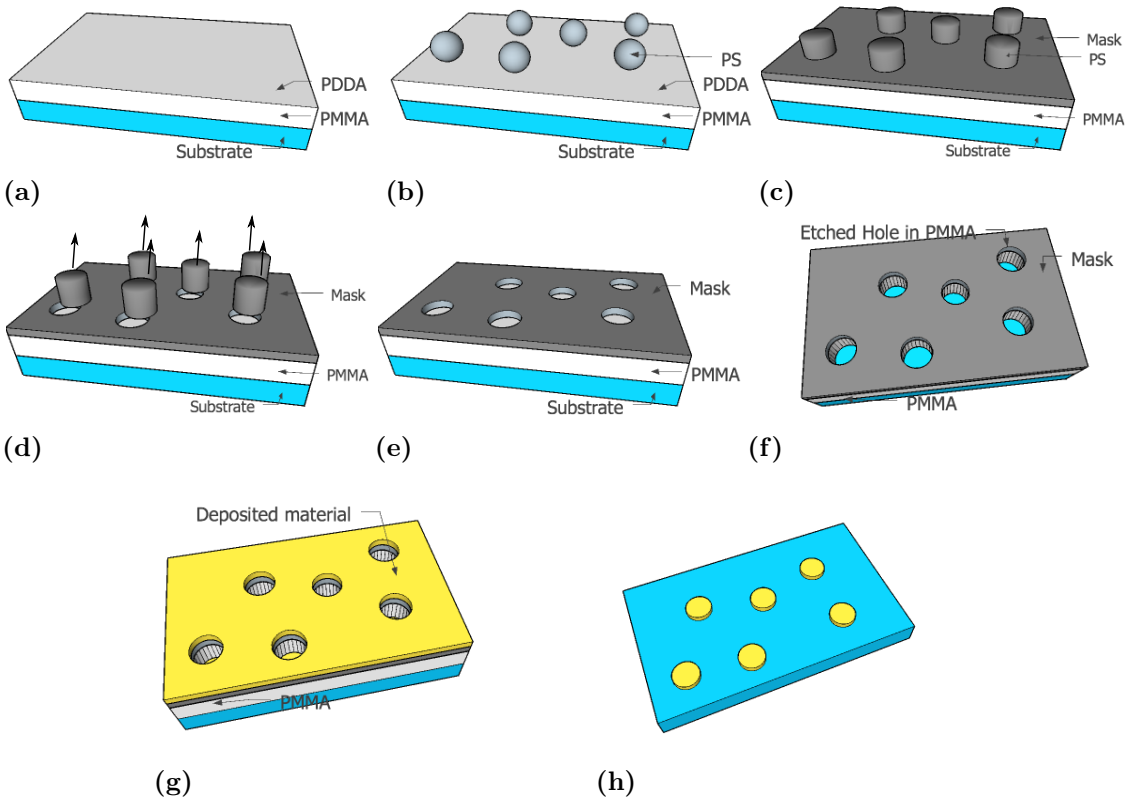


Figure 3.1: Steps for fabrication of mask for using HCL. **a)** PMMA is spincoated on a substrate and PDDA is applied to charge the surface. **b)** A solution containing PS spheres with opposite charge to the surface is applied. **c)** A metal film is evaporated on top. **d)** Using tape the covered PS spheres are removed. **e)** Left is a metal mask with holes. **f)** The PMMA is etched away leaving holes down to the substrate surface. Note that the substrate is seen in blue through the holes. **g)** Gold is evaporated through the hole. **h)** The PMMA is dissolved with acetone and everything attached to it is removed leaving only the structures deposited directly on the substrate.

9 Evaporation By evaporating different materials through the holes, structures are formed on the substrate surface. For my purposes I mostly used Shrinking-hole colloidal lithography which is explained bellow. In fig. 3.1g Evaporation of Au at an angle through one of the holes is presented.

10 Lift-off After completing the evaporation the mask is removed by dissolving the PMMA using acetone. This results in removal of all material that is attached to the PMMA layer, leaving only the material that is deposited directly on the substrate. See fig. 3.1h

11 Further etching steps Depending on the materials used, further etching can be performed on the substrate. This could, for example, be to remove sacrificial materials deposited on the surface for a specific reason.

3.2.5 Shrinking-hole colloidal lithography

A method based on HCL was developed recently and is called Shrinking-hole colloidal lithography (SHCL)[23]. The method utilizes the fact that as material is deposited through the mask it is also deposited on top of the mask. As the material is deposited on top it also builds up on the inside of the hole causing the hole to shrink. In fig. 3.3a a hole mask with deposited material is shown to illustrate how the hole shrinks. By depositing sacrificial materials on purpose the size of the hole can be controlled. In combination with the ability to tilt and rotate the substrate during material deposition this enables even more complex combination of structures to be fabricated. Disk-shaped structures can be evaporated onto the substrate by directly evaporating through the hole. The position of the deposited disk can be controlled by varying the angle of material deposition. In fig. 3.2 the angle needed to deposit a disk with a distance of D_1 from the center requires a tilting angle α that can be calculated as:

$$\alpha = arctan\frac{D1}{\sum T} \tag{3.1}$$

where $\sum T$ is the total thickness of layers above the substrate.
Using this in combination with the ability to shrink the hole, complex structures consisting of many different shapes can be made. In fig. 3.4 a cross-section of a trimer deposition with the shrinking hole mask on top is shown. The angle at which the hole shrinks depends on different parameters such as angle of deposition and the type of material. For example Cr shrinks the hole faster than Au as illustrated in fig. 3.4 where the angle at which Cr(grey) shrinks the hole is different from the angle seen for Au(yellow).
Deposition of sacrificial material to shrink the hole can be done in different ways depending on the requirements. The simplest way is to deposit the sacrificial material directly after the previous material using the same angle[23]. The result will be a cone deposited on top of the underlying material. This cone can later be removed using an etchant that only etches the sacrificial material. This method works if the materials wanted in the final structure are resistant to the etch used to remove the sacrificial material. For example Au and palladium can be used together with Cr as sacrificial material if the etchant used is selective to only removing Cr and not Pd and Au. To be able to use a wider set of materials different methods that do not require additional wet-etching steps have to be used. One of the main goals of this thesis was to develop and evaluate one such method called the “funnel method”.

3.2.5.1 *Cr funnel*

Another method for shrinking the hole is to deposit material using a high angle and continuous rotation[23]. This creates a “funnel effect” as the hole shrinks. The idea is to deposit the sacrificial material on the PMMA walls instead of on the substrate. This is illustrated in fig. 3.3b where Cr is deposited through the hole while rotating the substrate resulting in material building up on the PMMA walls and on top of the mask. During the removal of the mask (lift-off) the sacrificial material will then be removed with the mask and no extra processing step, such as wet-etching is necessary. The material for shrinking the hole can be chosen at will, in this thesis Cr was used because it shrinks the hole quite

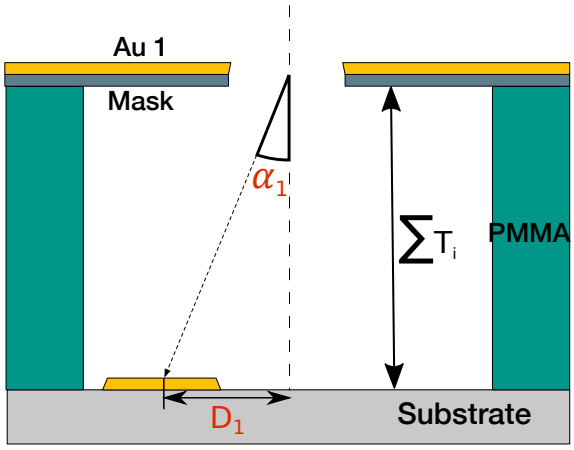


Figure 3.2: Sketch with indication of parameters used to calculate the angle for placing structures at desired places.

quickly, it is available and relatively cheap. The method makes it possible to use a larger number of materials that would not work with Cr-etch, such as Cu.

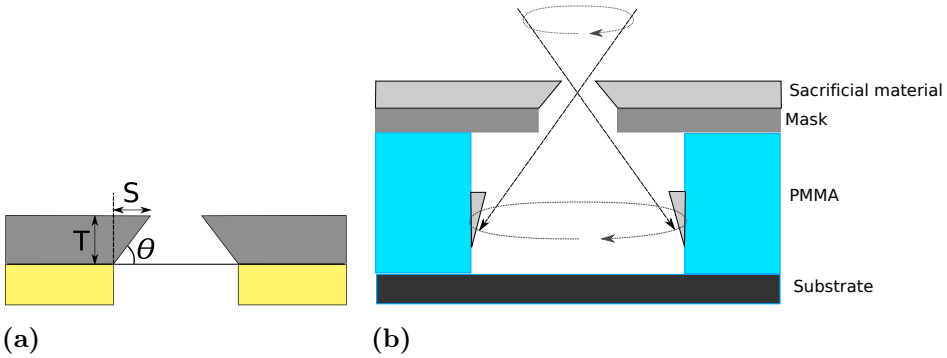


Figure 3.3: The process of controlling the shrinking of the hole in the mask for SHCL. **(a)** Schematic of how the deposited material grows inward resulting in a shrinking hole. Θ is the so called shrinking angle, T is the thickness of deposited material and S is the change in hole radius. **(b)** Schematic illustration of evaporation through hole mask using the funnel method.

Many factors determine the shrinking rate of the hole, the main ones are: tilt angle, evaporation rate and material. The rate at which the hole shrinks in respect to the amount of deposited Cr was empirically calculated as a shrinking angle. In fig. 3.3a the shrinking angle Θ is presented together with the thickness of deposited material T and the change in hole radius S that are used to calculate the shrinking angle.
Fig. 3.4 shows a schematic drawing of a cross-section for deposition of a Au trimer with a Pd particle using the SHCL funnel method. In the image, the deposited particles are seen as well as the growing mask on top of the PMMA. The Cr is deposited using an angle high enough so that it misses the substrate and instead grows on the PMMA walls. Due to the shrinking of the hole the order of deposition should be to begin with the largest and finish with the smallest structure.

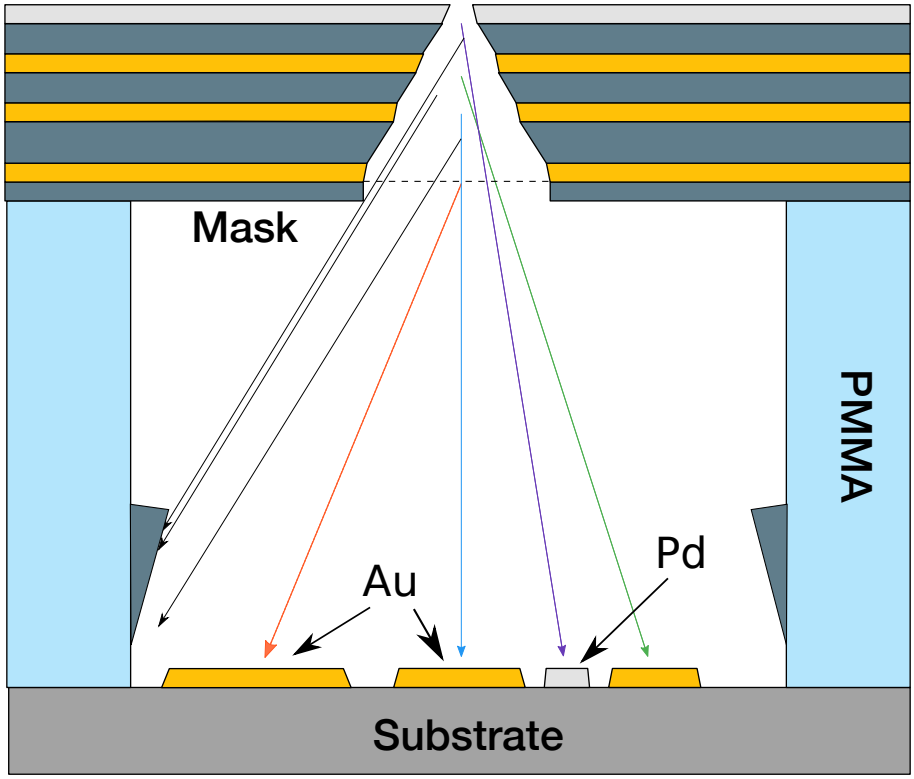


Figure 3.4: Illustrative example of trimer deposition through the hole mask using SHCL funnel method. The arrows symbolize evaporation paths for the materials that are evaporated at different times through the mask. Here three Au disks have been deposited followed by a palladium disk. Between each disk, chromium has been deposited to shrink the hole to the desired size. The Cr is deposited using a high angle resulting in Cr covering the PMMA walls instead of the substrate. The Cr evaporation is done during continuous rotation also illustrated in fig. 3.3b.

4

Characterization methods

The ability to characterize nanosized objects has improved dramatically over the last decades. Today there are methods available that make it possible to visually distinguish single atoms and determine information about compositions of particles of the size of nanometers. This chapter explains the main methods used for characterizing nanoparticles in this thesis.

4.1 Optical spectroscopy

To measure the optical response of plasmonic nanoparticles different optical spectroscopy methods are used. The main one was transmission spectroscopy where light in the near infrared (NIR) - visible(vis) - Ultra Violet(UV) region was used. In transmission spectroscopy light is shone through a sample containing nanostructures, and the attenuated signal is then collected using a detector, typically equipped with a grating to allow wavelength-dependent analysis.

Transmission measurements were done both for samples under steady-state conditions (in air at room temperature and pressure) and also during reactions where the surrounding conditions changed. The two different measurements require different types of instruments to get essentially the same type of information.

When doing the measurements under non transient conditions a UV-VIS-NIR spectrometer (Varian Cary 5000 UV-VIS-NIR) was used. This spectrometer measures the spectrum by scanning through the different wavelengths of choice one at a time. Inside it has a white light source that is made monochromatic using a grating monochromator, and the detector records the light intensity at every wavelength. Because this type of spectrometer only measures one wavelength at a time it takes a couple of seconds to scan the whole range of wavelengths investigated. For the transient measurements a complementary metal-oxide semiconductor (CMOS) array detector that has the ability to read the whole spectrum at every time-step was used to get a good time resolution of the spectrum. This type of detector uses a grating to send different wavelengths of light to different pixels of a CMOS detector. The detector then counts the number of photons corresponding to each wavelength. For both methods the amount of light that traveled through the sample compared to a reference value is measured. The transmission is defined as:

$$T = \frac{I}{I_0} = 1 - E = 1 - (S + A) \tag{4.1}$$

where I is the intensity measured at the detector, I_0 is the reference intensity, E is the

extinction, S is the scattered light and A is absorbed light. The reference intensity is the intensity of light that reaches the detector when a sample without any nanoparticles is placed in the light path.

4.1.1 Polarized light

Polarized light was used to measure the effects of direction of exciting light on the fabricated structures. For the measurements performed in the Cary spectrometer a polarization filter was placed in the light path. For the transient measurements with the CMOS detector, a beam-splitter was placed after unpolarized light interacted with the samples. The beam-splitter separated the light polarized along and parallel to the structures, enabling measurements of both spectra simultaneously. The beam splitter is connected to the optical exit path of the reactor as illustrated in fig. 4.1. Structures with certain asymmetries are expected to interact with light differently depending on polarization. For a structure illustrated in fig. 2.3b, the change of the small particle (to the right) is proposed to give rise to a larger change in the plasmonic response of a big antenna particle (to the left), if the light is polarized parallel to the structure axis rather than with the light polarized perpendicular to it. Therefore the perpendicularly polarized light can be used as a reference measurement to single out changes not related to the particle of interest. This method of using polarized light as a reference has been demonstrated for a Au-Pd heterodimer for detection of hydride formation of Pd[34].

4.2 Scanning electron microscopy

Scanning electron microscopy (SEM) is a microscopy technique used instead of optical microscopy to be able to distinguish smaller features than what is possible using visible light. In the SEM the substrate is bombarded with a focused beam of electrons created in an electron gun. Depending on the material of the underlying substrate, the electrons interact with it in different ways. The main events that occur are: elastic backscattering, generation of secondary electrons and generation of electromagnetic radiation (x-rays) due to retardation of incident electrons and from relaxation of excited states in the imaged material.

To create an image of the material, mainly the secondary electrons and the backscattered electrons are used. The contrast in the image from backscattered electrons comes from the fact that heavier atoms scatter electrons more efficiently than lighter ones. This creates an image where heavier atoms appear brighter than lighter atoms. Secondary electrons are generated when electrons are ejected from the high energy shells of atoms as a result of the electron bombardment by the electron beam. These electrons can be ejected from a few nm bellow of the sample surface.

Because the substrate is bombarded by charged electrons the surface will be charged during imaging. To prevent accumulation of charge the substrate should be conducting. This criteria limits the substrate material that can be used for imaging in SEM. For example glass does not work because it is an insulator. Therefore, in this thesis, glass and Si substrates

with nanostructures were fabricated in parallel, to enable both transmission measurements and SEM imaging of structures fabricated under identical conditions.

4.3 Hydrogen sensing

Hydrogen sensing was used as a method to assess the sensing performance of some of the plasmonic structures developed in this thesis work. This was done because it is a well studied as well as reversible phenomenon, on structures similar to those fabricated within this thesis. The experiments took place in a small chamber with the possibility to evacuate air down to a pressure of a few Pa. A gas inlet was connected to this chamber, with the possibility to introduce H_2 in a controlled manner. The chamber also had the possibility to control the temperature in the range from room temperature up to a few hundred degrees Celsius. An optical pathway through the chamber made it possible to measure an optical extinction spectrum of the substrate inside in real time. A light source and a detector were connected to the chamber through optical fibers. A beam splitter acting as polarizer was connected to the outlet of the chamber making polarization dependent measurements possible.

4.4 Oxidation and reduction experiment setup

Experiments to investigate the effect of oxidizing and reducing environments on metal nanoparticles took place in a commercial reactor called X1 manufactured by the company Insplorion. This reactor has the possibility to control mass-flow of gases, such as H_2 and O_2, and temperature in the reactor. Light source and detector(s) where connected to the reactor by optical fibers. By adding a polarizing beam splitter to the optical output of the reactor the different optical response depending on polarization could be measured. Figure 4.1 shows a schematic image of how the X1 reactor looks like and the important components are marked.

4.5 Single particle spectroscopy

Measurements of the optical properties of single structures where made by measuring their scattering spectrum. The setup to do this consisted of an optical microscope equipped with a reaction cell with the possibility to control temperature and gas composition. A CCD based spectrometer connected to the microscope was used to gather the scattered light from a circle with a dimater of about 12um on the substrate. Illumination of the samples was done using reflected-light dark-field mode in the optical microscope. This means that the sample is illuminated from the sides and only the scattered light (perpendicular to the illumination) is collected by the detector. This method of measuring dark field scattering spectra is known as dark-field scattering spectroscopy. By doing this instead of looking at

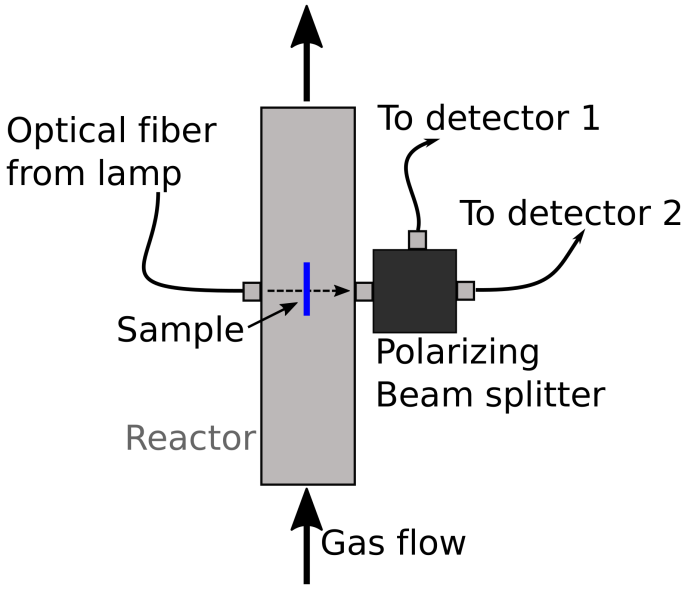


Figure 4.1: Schematic image of the X1 reactor setup used for transmission spectroscopy of nanostructures at different temperatures and gases. Here a polarizing beam splitter is mounted to enable measurements of two polarizations of light simultaneously.

transmitted light as for the ensemble measurements, data from much smaller samples can be collected.

The structures of interest where found using dark field mode in the microscope making scattering species, such as particles with LSPR, visible as bright spots against a dark background. An example of how finding a good particle in the SEM, mapping its position and then finding it again in the optical microscope is shown in fig. 4.2. In section 4.5 a good candidate structure is first found with SEM imaging. Its specific geometrical properties can be recorded. Following this a map of the substrate surface is created by stepwise zooming out (sections 4.5 to 4.5). Later, the correct structure can be found in the optical microscope by following the map created in the SEM. The correct structure is marked with an arrow presented in section 4.5).

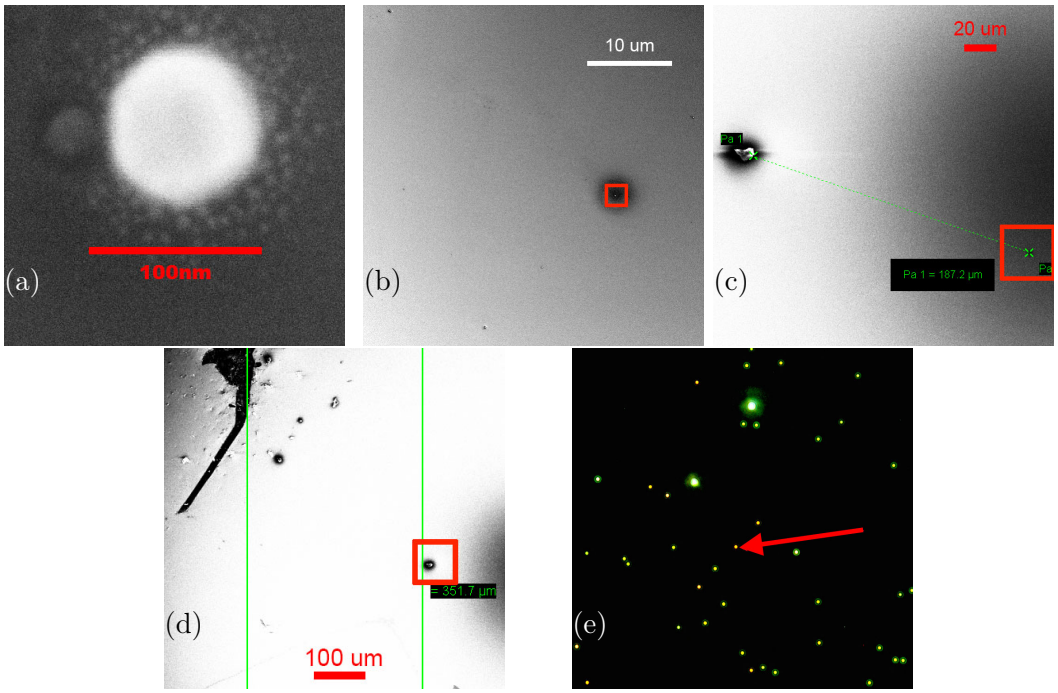


Figure 4.2: Method used for mapping a structure in the SEM to later be able to find the same structure in the optical microscope. Red squares indicate the area which corresponds to the previous picture. **(a)** My structure imaged in SEM. The big white circle is a Au disk 100nm in diameter 50 nm thick. The smaller grey dot is the Cu disk 30 nm diameter and 20 nm thick. **(b)** The near surroundings of my particle. **(c)** Distance between structure and a larger piece of dirt to the left marked. **(d)** SEM image zoomed out, in the upper left is a scratch visible by the eye. **(e)** Image of particle in dark field microscope.

5

Fabricated structures

In this chapter fabricated nanostructures are presented together with results related to the fabrication process.

5.1 Fabrication of plasmonic trimer

Trimer structures consisting of three Au nanodisks with decreasing size were fabricated using SHCL described in section 3.2.5. The specific geometry of the trimers was chosen based on the self-similar antennas presented in the literature[10]. A Pd particle was placed in the hottest spot of this structure which is in the gap between the two smallest Au disks. The goal was to investigate the possibility to make advanced plasmonic nanostructures using SHCL funnel method without the need of additional etching of the substrate surface. The Au Pd system was chosen because the interaction between H_2 and Pd is a well studied system and the expected plasmonic response from similar structures has been studied before. To verify the fabrication method the made structures were investigated in different ways. First, the structures were imaged in a SEM and visually inspected and structural parameters were compared to the planned ones. Distances and sizes were measured using the scientific imaging tool ImageJ[35] and the structures imaged in the SEM were randomly chosen to try to get a non-biased sample-volume.

5.1.1 Evaluation of fabricated structures

The first purpose of the SEM images was to see if the structures had the right features. Due to the possibility of many errors during fabrication of the structures some samples turned out wrong. An example of a failed structure where the three Au disks overlap instead of being separated as intended is presented in fig. 5.1. The overlap was in this sample due to a too thin PMMA layer during the fabrication of the mask. This resulted in deposition angles that were too small and the resulting disks ended up on top of each other.

5.1.1.1 *Cr funnel method*

Deposition of sacrificial material through the hole in the Cr mask results in shrinking of the hole. To quantify how much sacrificial material that has to be deposited, a closing angle is determined from measurements on the final structures. The funnel method of SHCL was

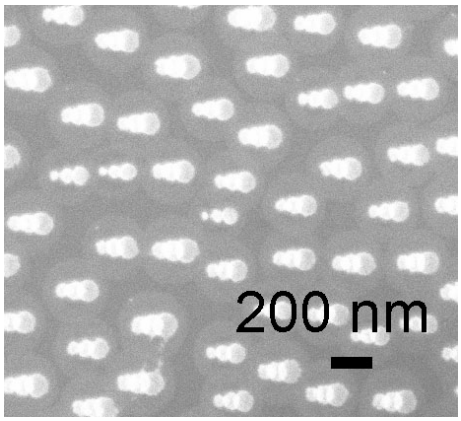


Figure 5.1: Failed trimer structures with overlapping Au disks.

based on previous work by Syrenova et.al.[9] and the model system was further optimized. To quantify the rate at which the hole shrunk, the amount of deposited Cr was used as a measure. The reason behind this is mainly because the evaporator can be set to evaporate a certain thickness of material. The relation between evaporated film thickness and the change in hole diameter was then calculated as a shrinking angle that was seen as the angle between the substrate surface and the mask wall described in fig. 3.3a in section 3.2.5.
By measuring the size-difference of the final structures the shrinking angle could be calculated and tuned for future depositions.

Shrinking hole The change in hole diameter depending on the amount of deposited Cr using the funnel is presented in fig. 5.2. It was presumed that the correlation of the parameters would be linear and a line fitted to the data showed quite good correlation. The line does not, however, go to zero when nothing is deposited. The reason behind this was determined to be due to a faster shrinking of the hole during the first few nm of deposition. The exact reason resulting in this is not fully understood but it can be related to the properties of Cr being deposited on top of a different material in comparison to being deposited on a underlying layer of Cr. The hole shrinking could then be expressed as:

$$\Delta D = 5.13 + 0.66 * T_{Cr} \tag{5.1}$$

where T_{Cr} is the thickness of the deposited Cr layer.

Cr Rings The main advantage of using the funnel method to deposit structures is that no chemical wet etching is needed on the final structure. To ensure no Cr was deposited on the substrate the samples were investigated using SEM. As a starting point, the angle used for the funnel was calculated so that no Cr would reach the surface as long as the evaporated Cr traveled in a straight line from the source through the hole.
In fig. 5.3 trimer structures are shown quite densely packed on the surface. To the right in the image ring-like white areas are seen around the trimers. These rings were determined to be Cr that had reached the substrate during the hole-shrinking. Because not all structures resulted in the ring structures the reason behind the rings was determined to be related to structural differences among the holes.

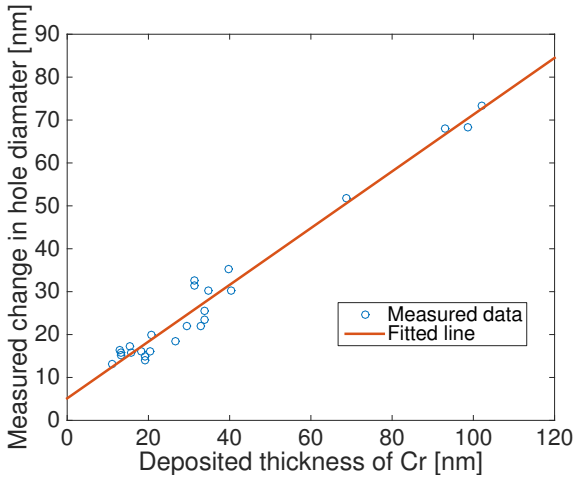


Figure 5.2: The change in hole diameter plotted against thickness of deposited Cr using the funnel method.

The first approach to get rid of the rings was to increase the evaporation angle used for the Cr funnels. This however did not solve the problem and the ring-like structures persisted. The next proposed cause for the problem was internal stress in the mask causing the holes to deform. It is known that high melting point metals like Cr tend to show a high intrinsic stress when deposited at a low temperature as a coating on plastics[36]. The stress can then result in cracks or buckling of the material, which in turn would affect the way the holes look, and change the deposition path later on in the process. To relieve the mask from stress, a lower surface coverage of PS was tested by decreasing the PS concentration during the mask fabrication. This did reduce the number of rings appearing on the substrate and with a low enough surface coverage all structures were ring-free. However, using a low surface coverage decreases the usability of the HCL method because a high coverage of structures is needed to be able to make good measurements of ensembles. Another proposed solution to relieve tension in the mask was to heat-treat the mask after deposition. This was done by placing the Cr-mask in an oven before the under-etching step using O_2 plasma. The heat would make the atoms in the mask more mobile and rearrangement of the atoms in the mask could result in a mask with less intrinsic stress. The result of this approach was both positive and negative. The good part was that the Cr-rings were almost completely removed in most parts of the sample surface. The downside was that large cracks formed on the mask. Where the cracks formed the plasma etching etched away all the PMMA down to the substrate surface resulting in deposition of material through the cracks effectively destroying the possibility to use the sample for ensemble measurements. In fig. 5.4 an image showing the sizes of the cracks together with an image of how the Cr-rings show up near the cracks but not on the areas far from the cracks. The conclusion of this was that the tension in the mask was relieved by breaking it into smaller pieces. However the method did not solve the problem.

The next approach was to use Au as mask-material instead of Cr. This was done because Au has a lower melting point than Cr and should therefore result in a mask with lower intrinsic stress[36]. This resulted in a more reliable mask without the Cr rings deposited on the substrate at a higher surface coverage than was possible using the Cr-mask. With a low

coverage of holes and using a Au mask successful structures without unwanted material deposited on the substrate could be fabricated. The surface coverage was high enough to enable transmission spectroscopy of the samples. An example SEM image of a few successful structures is presented in fig. 5.5.

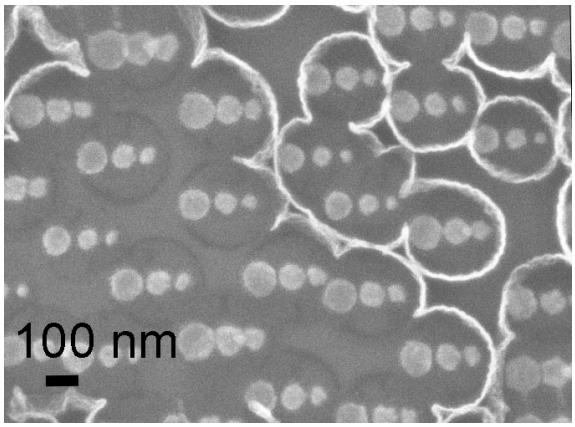
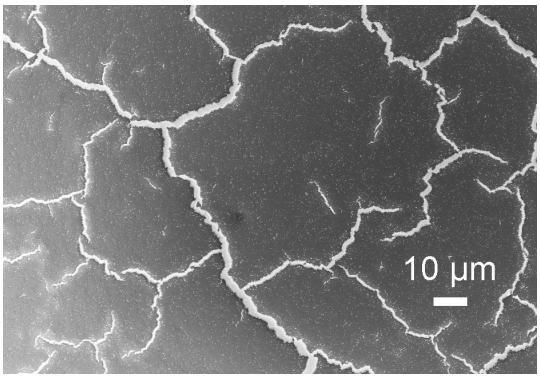


Figure 5.3: Trimers fabricated using the SHCL funnel method. Cr is seen as white depositions around the trimers.

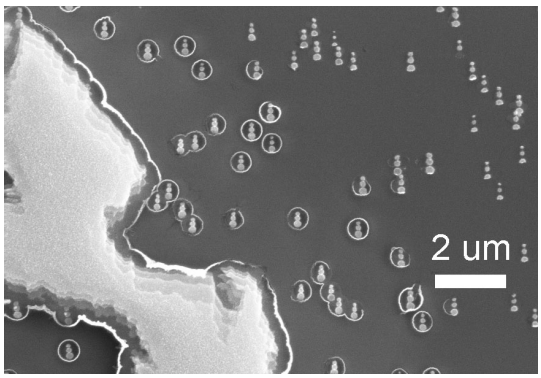
5.2 Au-Cu structures for indirect sensing of oxidation and reduction of metal nanoparticles

The SHCL funnel method was used to fabricate structures consisting of a single Au disk with a smaller Cu particle placed beside it. The fabrication steps were the same as for the trimers explained above but with fewer evaporation steps. These structures were fabricated both for application in ensemble measurements and for single particle spectroscopy.
The ensemble structures were made using a 100 nm PS solution with concentration of 5e-4wt% following the recipe described in section 3.2. Four typical Au-Cu structures imaged using SEM directly after fabrication are presented in fig. 5.6a. As discussed in previous chapters the fabrication parameters had to be tuned to avoid unwanted Cr deposition on the substrate. In fig. 5.6b a structure with some Cr deposited around it can be seen to the right. Closer inspection shows that this structure was formed by two PS beads dimerizing and therefore creating a larger hole than wanted in the hole mask. This larger hole resulted in a larger under-etch of the PMMA. A large hole in combination with more under-etch makes the probability of Cr ending up on the substrate larger. The fabricated samples all had some of these failed structures but it was determined they were so few so the average effect of their presence was negligible.

Single particle samples For the single particle samples a similar fabrication method was used with the only difference being the concentration of PS and application time of the PS before rinsing. To be able to measure the scattering spectrum of a single structure there has to be a certain nearest neighbor distance between each structure. For the particular setup used for single particle measurements the minimum distance between adjacent structures



(a) Cracks in PMMA resulting in material deposited in crack-like shapes on the substrate



(b) Zoomed in image of crack in the bottom left, showing that Cr-rings are formed around structures close to cracks but not far away from the cracks.

Figure 5.4: SEM images showing crack formation due to annealing of the mask during fabrication.

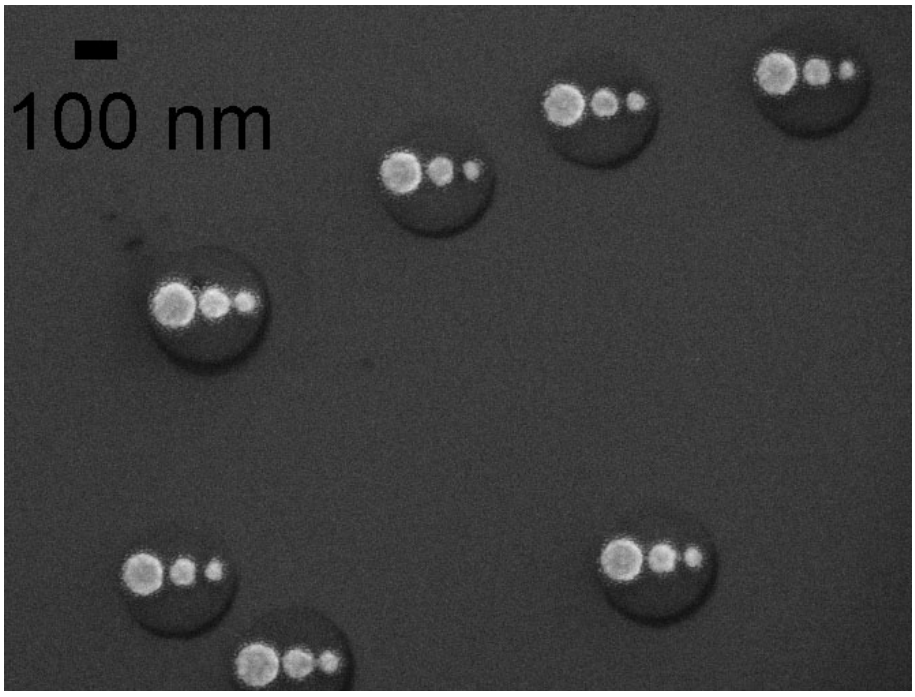
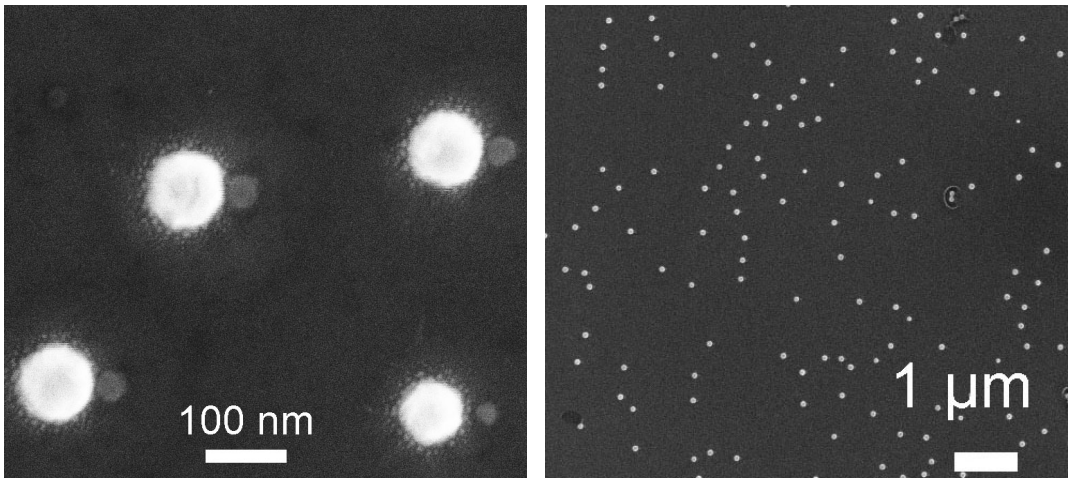


Figure 5.5: Trimers fabricated using Au mask and low PS coverage.



(a) Four example structures showing the size distribution among structures

(b) The typical surface coverage of the sample. Seen to the right is a structure that has a Cr ring which is a typical problem with SHCL and the funnel method

Figure 5.6: Structures consisting of Au disks with a size of 100×50nm (Diameter×height) and copper disks placed to the right with the size 30×20nm. The samples were fabricated for ensemble measurements using transmission spectroscopy.

was 24 um. This distance was achieved by using a PS solution concentration of $0.5 \cdot 10^{-4} wt\%$ and an application time of 20 s before rinsing.

5.3 Effects of annealing

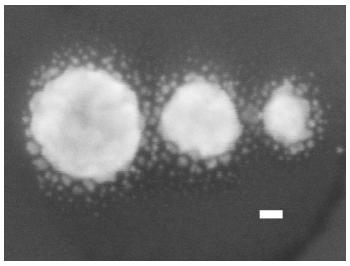
The effect of annealing the structures and the resulting effects on the optical properties of the samples were investigated. The first reason the annealing was used was to make the structures more homogenous. Annealing of similar disk-like structures made of Au has previously been shown to cause the disks to become more spherical causing the plasmonic peak to become narrower and blue-shifted[37]. Heating Au nanoparticles will make the Au atoms more mobile and they are expected to rearrange themselves to a more thermodynamically stable shape.

Annealing trimer structures for 2h in 350°C resulted in both structural and optical changes shown in figs. 5.7a and 5.7b. The shape of the Au disks became more circular and the small particles surrounding each disk disappeared, probably due to them merging with the larger disk. By measuring the disks, averaging and comparing the sizes before and after annealing a change in size was also seen. The results on several structure parameters is presented in table 5.1

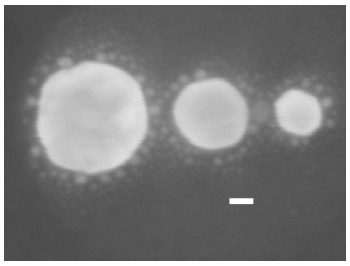
It can be seen that the diameter of all the Au disks decreased and as a result the distance between the disks increased. Also the standard deviation between disk sizes decreased after annealing indicating a more narrow size distribution.

Table 5.1: Effects of annealing at 350°C for 2h on Au trimers. D_i is diameter of disk i and $d_{i\leftrightarrow j}$ is the edge-to-edge distance between disk i and j. The column value shows the average measured value of the specific parameter and Stdev is the standard deviation among the measured samples. The data was gathered from 10 randomly selected structures before and after annealing.

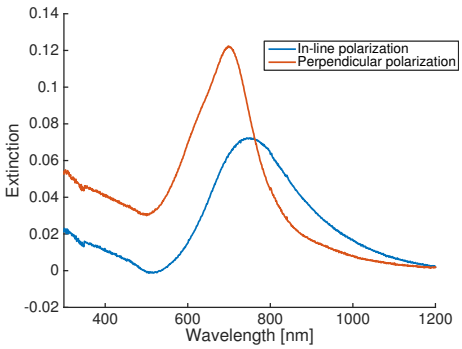
	Before annealing		**After annealing**	
	Value [nm]	Stdev [nm]	Value [nm]	Stdev [nm]
D_1	106.0	5.2	95.1	3.6
D_2	73.4	6.7	57.1	4.4
D_3	49.0	5.8	35.8	4.8
$d_{1\leftrightarrow 2}$	15.6	5.9	26.7	8.5
$d_{2\leftrightarrow 3}$	21.3	5.5	28.7	5.0



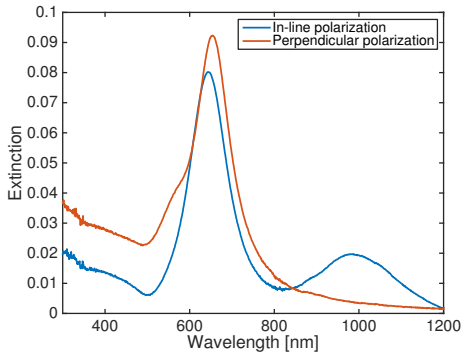
(a) SEM image of trimer structure



(b) After anneal



(c) Before anneal



(d) After anneal, 350°C 2h

Figure 5.7: SEM images and optical extinction spectrum of trimer structures before and after anneal. The scale bars in the SEM images represent 20 nm.

6

Results

This chapter presents and discusses the results obtained from optical measurements of the plasmonic nanostructures that were fabricated.

6.1 Trimers for H_2 sensing

Images taken in the SEM were used to verify the fabricated surface coverage and that the structures looked as expected. In the early fabrication stages they were also used to fine-tune the fabrication parameters such as the angles and the rate of hole shrinking, see section 3.2.5.
In fig. 5.7a a typical trimer structure is presented. This structure shows the correct placement of the Au disks without overlap. The Pd particle that is supposed to be placed between the smallest and the second smallest Au disk is hard to see due to the low contrast of Pd compared to Au in the SEM.

6.1.1 Optical spectrum

Extinction spectra of the fabricated structures were measured to verify the plasmonic peak. The spectrum after anneal of the samples was also measured to see if the desired narrowing of the plasmonic peak was achieved. In figs. 5.7c and 5.7d the extinction spectrum for different polarizations is presented before and after anneal of the structures. The narrowing of the peak indicates that the structures have become more homogenous and that every disk has a more spherical shape. This was also verified by comparing the structures before and after anneal in SEM. In fig. 5.7b the more circular shape compared to the image before anneal is visible.

6.1.2 Hydride formation

The finished trimer structures without Cr-rings were placed in the vacuum chamber for H_2 storage experiments. Here the plasmonic response of the structure due to changes in H_2-pressure was measured at constant temperature. Previous experiments on similar Au-Pd based structures have shown that light polarized in-line with the structures shows a larger response to changes in the Pd particle[23,34]. Therefore the spectrum was measured using

light polarized in line with the trimer structure and peak characteristics (peak wavelength, intensity, FWHM) were found by fitting a Lorentzian function to the acquired spectra.

The change of the peak wavelength in response to changes in H_2-pressure at constant temperature of 20°C is presented in fig. 6.1. This measurement shows the typical hysteresis of H_2 storage in Pd, as shown in several previous experiments[3,5,34].

This shows that fabricating complex structures with precise placement of particles down to a size of around 15 nm is possible using SHCL funnel method. I believe that further tuning of the structural parameters could enable sensing of even smaller particles both in ensemble and single particle measurements.

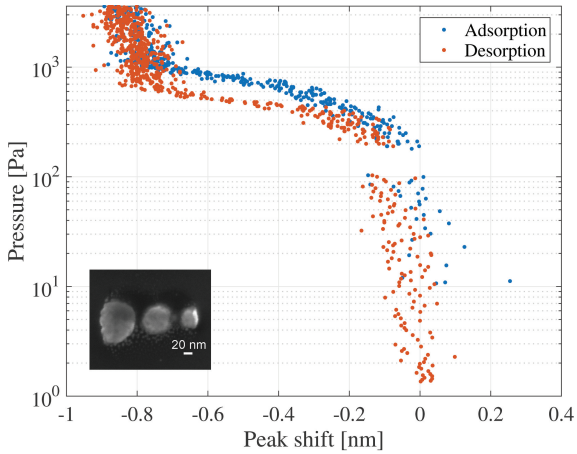


Figure 6.1: Peak position of trimer structures with a 15nm Pd particle in the hottest spot under varying H_2 pressure. The typical hysteresis for adsorption and desorption is clearly visible. Inset shows SEM image of typical trimer structure.

6.2 Indirect sensing of oxidation and reduction of Cu nanoparticles

Au-Cu structures were fabricated using the SHCL funnel method. The optical response of the nanostructures to an oxidizing and reducing gas-flow at different temperatures was investigated. The measurements of ensembles with Au-Cu structures were conducted using both unpolarized light and light polarized as parallel (in-line) to the structures and perpendicular to the two structures as shown in fig. 6.2. The idea was that due to coupling between the plasmonic modes of the Cu and the Au, changes occurring only in the Cu should be more visible in the polarization direction in-line with the axis that connects the two particles. The perpendicular signal can be used as reference measurement, making it easier to single out the changes related to the Cu. Extinction spectra measured on newly fabricated samples consisting of Au-Cu dimers are presented in fig. 6.2 for the two polarization directions indicated. It can be seen that light polarized in-line with the two disks has a broader plasmonic peak and is red-shifted compared to the polarization perpendicular to the structures.

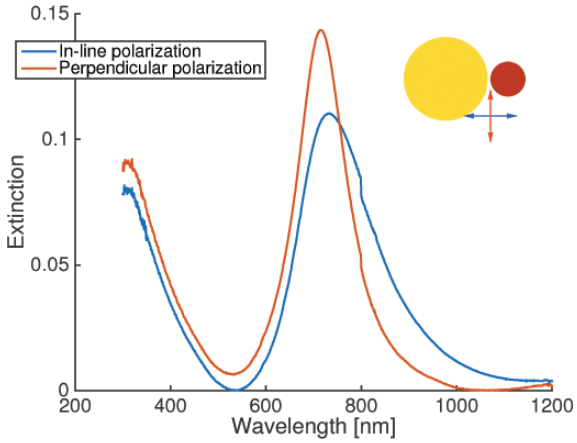


Figure 6.2: Extinction spectra of Au-Cu structures for two polarizations of light. Blue is the light polarized parallel to the two disks and red is from light perpendicular to them. To the right is a sketch of a typical structure with the polarization directions represented with colors. The two polarization directions are also indicated by arrows below an inset illustrating the Au-Cu structure in the top right.

6.2.1 Plasmonic response using unpolarized light

Measurements of optical changes of a Au-Cu dimer when exposed to O_2 and H_2 at different temperatures were made in the X1 reactor described in section 4.4. The structures used were Au disks 96 nm in diameter, 50 nm thick and Cu-disks 30 nm in diameter, 20 nm thick placed at about 5 nm from the Au on a borosilicate (borofloat®) glass substrate. The spectrum was collected as an average of every 5 second interval together with the corresponding mass-flow rate and temperature. A Lorentzian function was fitted to the collected spectra at every time-step to get the peak characteristics: peak wavelength, extinction intensity at the peak and FWHM of the peak. The effects on the plasmonic peak wavelength during a constant gas flow of 100 ml/min while alternating between 2% O_2 and 4% H_2 in Ar are presented in fig. 6.3. This was done at temperatures above and bellow when reduction and oxidation of the Cu nanoparticles was expected to occur according to previous sources[31,38]. Here, a clearly reversible behavior of the peak position can be seen when the structure is exposed to H_2 or O_2. O_2 exposure results in a red-shift of the peak and H_2 – a blue-shift. Higher temperatures increase the amplitude of the shift and also makes the transition speed higher. To better visualize the oxidation and reduction behavior of the system the response to the two gases was individually explored.

6.2.1.1 *O_2 response*

In fig. 6.4 the change of the peak position when 2 % O_2 is introduced at different temperatures is shown. Each O_2-introduction was repeated three times at every temperature and each line-color represents a certain temperature. In fig. 6.4a the larger peak shift at higher temperatures is clear. To be able to identify different reaction steps more clearly the time was plotted as a log-scale in fig. 6.4b. From this figure it is possible to identify four different

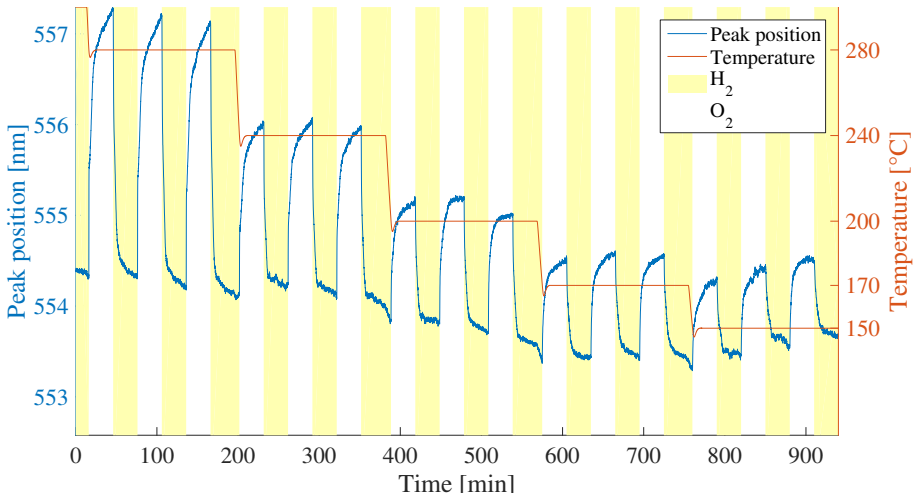
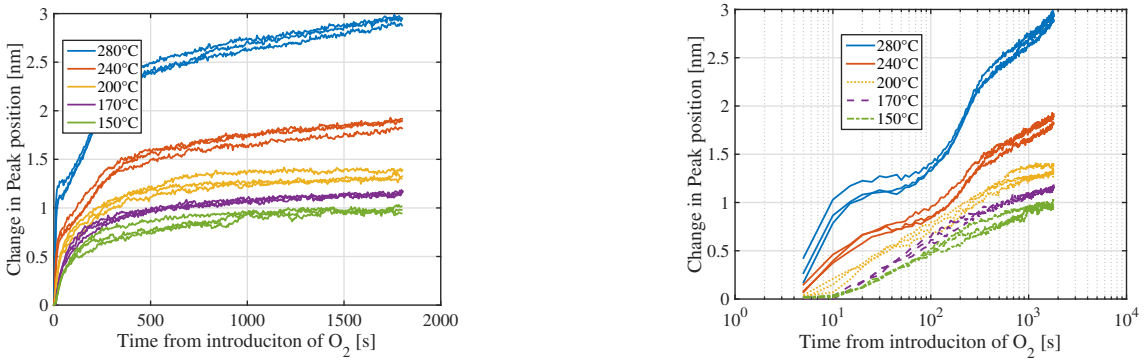


Figure 6.3: Peak position response of alternating H_2 O_2 cycles at different temperatures. Yellow shaded areas correspond to 4% H_2 and the white areas 2% O_2, both in Ar.



(a) **(b)** Logarithmic time scale

Figure 6.4: Plasmonic peak change of a Au-Cu structure as 2% O_2 is introduced. All peak positions are moved to 0 at the introduction time. Colors represent different temperatures and repeated lines are separate experiments.

regions of reaction rates which are easiest to identify by looking at the 280°C plot. The first quick change in peak position is during the first 20–30 s and it is followed by a slow change period until the 100s mark. After around 100s the rate of change increases again until 200–300 s, where slowdown in the rate of change is seen. For temperatures bellow 200°C the initial jump in peak position is not seen at all. Instead, a seemingly constant slope for the rate of change in the log-plot is seen until about 500 s, where the change of peak position slows down.

The predicted reactions taking place in Cu when exposed to O_2 in the temperature range (20–300°C) investigated are[31]:

$$2Cu + 0.5O_2 \rightarrow Cu_2O \tag{6.1}$$

$$Cu_2O + 0.5O_2 \rightarrow CuO \tag{6.2}$$

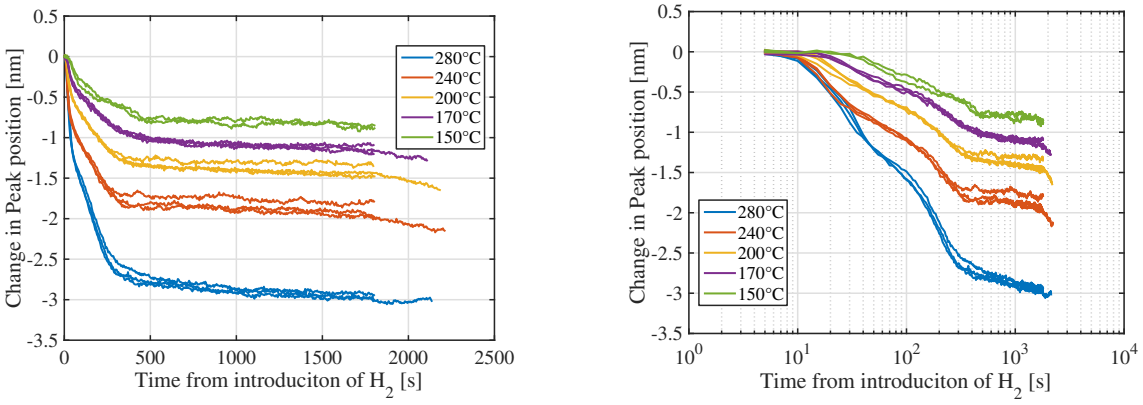
$$Cu + 0.5O_2 \rightarrow CuO \tag{6.3}$$

and the different reaction rates are proposed to be related to these three reactions. It is,

however, also probable that other reactions related to the substrate and the Au surface have an impact on the plasmonic response when exposed to H_2 and O_2 as has been shown in previous studies[39,40].

6.2.1.2 *H_2 response*

To reduce Cu, 4% H_2 in Ar with a flow-rate of 100 ml/min was introduced for 30 minutes at different temperatures. The resulting response of the plasmonic peak position is presented in fig. 6.5. Similar to the "oxidations", it can be seen that the amplitude of the peak shift is larger at higher temperatures. In the log-scale, 6.5b, it is possible to identify regions of different reaction rates when the sample is placed in a reducing environment. During the first 10–20 s there is no change of the peak position for any of the temperatures. After the initial delay, a blue-shift is seen for all temperatures and a higher temperature results in a quicker change. For temperatures above 200°C a slow down in the change rate is seen after about 20 s. Between the 100–200 s mark another increase in the change rate is seen for all of the temperatures. For all temperatures except 280°C the change in peak position flattens out after 200–500 s. For 280°C the peak position continues to drift after the distinctive slow-down of change rate at around 300 s. After this time the reduction is presumed to be complete. The reduction of copper oxide is proposed to result in a change in the plasmonic peak, but as for the case of oxidation, other reactions have shown to occur on the substrate surface of similar systems or on the Au itself resulting in changes of the plasmonic properties[39–41].



(a) **(b)** Logarithmic time scale

Figure 6.5: Plasmonic peak change of a Au-Cu structure as 4% H_2 is introduced. All peak positions are moved to 0 at the introduction time. Colors represent different temperatures and repeated lines are separate experiments.

6.2.2 Polarization dependence

There are many potential reactions that could occur in/on the substrate when exposed to different atmospheres, for example H_2 spillover has been shown to generate a measurable change in the plasmonic signal of Au nanorods on metal oxide supports[41]. To better

capture the effects taking place in the Cu particle and at the same time being able to ignore changes in the substrate and the Au disk, polarized light was used. It has been previously demonstrated that coupling between Au disks and Pd particles results in a larger plasmonic peak shift in the polarization direction parallel to the two structures compared to the perpendicular direction[34]. The polarization directions used in this thesis were the ones described above and presented in fig. 6.2. The idea was that the coupling between the Au and Cu disks should be stronger in the polarization in line with the two particles, therefore changes taking place in the Cu due to chemical reactions was expected to have a larger impact on the signal measured in-line compared to the one perpendicular to the structures. The perpendicular polarization measurement was therefore proposed to be used as a continous baseline measurement to correct for drift in the signal corresponding to "unwanted" reactions and temperature changes.

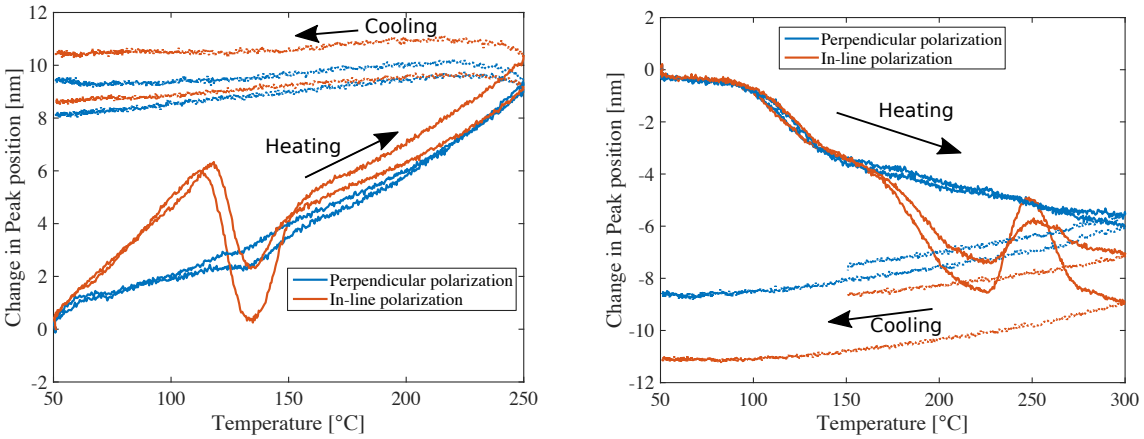
The structures used for these measurements consisted of an Au disk with average dimensions 94×50 nm and a Cu disk (40x30 nm) placed 5 nm from the Au and on a fused silica substrate coated with a 50 nm thick silicon nitride layer. The change of substrate materials was done to see if any substrate effects could affect the measurement.

6.2.2.1 *Temperature ramps*

To investigate at what temperature the small Cu particles oxidized and reduced, the system was placed in an O_2 or H_2 environment during temperature ramps. The temperature was increased at a rate of 5°C/minute starting at 50°C and increasing to a maximum of 250°C for the oxidation and 300°C for reduction.
All temperature ramps were followed by a cool-down under which no significant change of the plasmonic peak was expected. Data for both heating and cooling is therefore presented to be able to exclude temperature related changes in the plasmonic peak.

O_2 response The change of peak position of the Au-Cu structure under constant flow of 100 ml/minute of 2 % O_2 in Ar during a temperature ramp from 50 to 250°C is presented in fig. 6.6a. In this figure it can be seen that the polarization in line of the two particles has a more rapid change rate from the start of the temperature ramp. At about 130°C there is a distinct blue-shift of the in-line signal, followed by a red-shift. At 150° the two channels have the same change rate and both continue red-shifting. In fig. 6.7a the difference between the peak position of the two polarization directions is presented during the temperature ramp in O_2. In the figure the two colors represent two separate measurements and heating and cooling is distinguished by solid and dotted lines respectively. From this figure it can be seen that the signal from the two polarization directions change in different ways from 50–150°C. This indicates that changes related to the small Cu-particle are taking place even at temperatures as low as 50°C. In the range 130–150°C the large blue-shift followed by a red-shift is clearly seen as a decrease in the peak position difference followed by an increase. Comparing to previous experiments done on single Cu-nanoparticles with similar size[42], the Cu is not expected to oxidize at temperatures bellow 125°C. Therefore the changes seen at lower temperatures are presumed to be due to surface reactions on the Cu-particle

that affect the resulting plasmonic properties of the system.



(a) Temperature ramps in O_2 **(b)** Temperature ramps in H_2

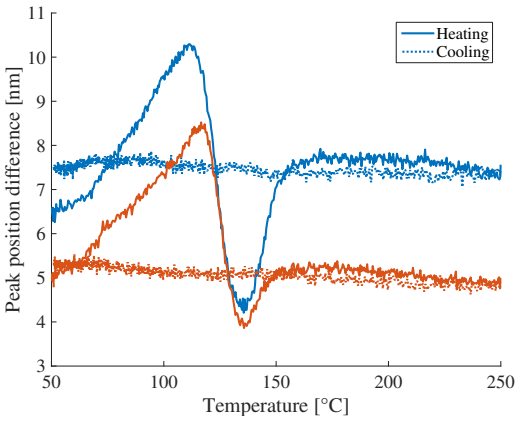
Figure 6.6: Temperature ramps of Au-Cu dimer structure under different surrounding gases. Values on the y-axis are of changes in peak position of the signal, where 0 is the peak position at the start of the temperature ramp. Solid lines represent the response during heating and dotted lines the response during cooling. Before each ramp in H_2 the samples were oxidized in O_2 during a temperature ramp and before O_2 they were reduced. Each ramp was measured two times.

H_2 response The response of the plasmonic peak position during temperature ramps at constant flow of 4% H_2 in Ar is presented in fig. 6.6b.

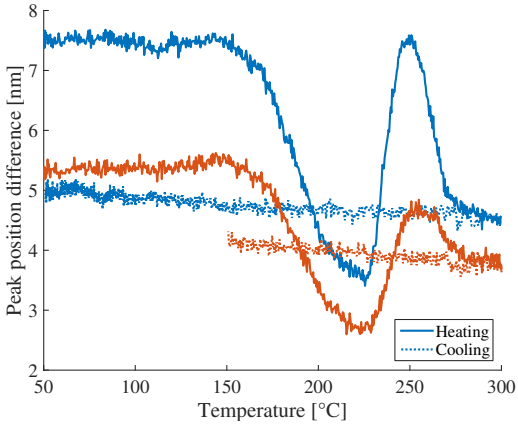
The change in the two signals starts to differ after 160°C when a blue-shift is seen in the polarization that lies in-line with the Au-Cu structure. The blue shift continues until 230°C when there is a red-shift until 250°C followed by another blue-shift. The two polarizations have the same change rate (slope) after 280°C up to the maximum temperature of 300°C where the cooling begun.

To single out the changes taking place in the Cu particle, the difference between peak positions of the two measured polarizations is presented in fig. 6.7b. In this figure two separate measurements of the same sample are presented distinguished by color. In this figure a constant value of the y-axis corresponds to the two peak positions changing at the same rate. A changing value means that the two peaks change in different ways indicating that something different is happening depending on which polarization of light that is used. During the cooling the peak positions are quite stable except a slight blue-shift for both channels that is assumed to be temperature related.

Discussion The large changes seen at 130°C for the oxidation and 160°C for the reduction experiment correlate well to previous identical measurements done on pure Cu nanoparticles with a slightly larger size (67×20 nm). In these measurements a quick disappearance of the plasmonic peak of Cu nanoparticles was seen at a temperature between 125–140°C[42]. During the reduction the plasmonic peak corresponding to Cu quickly reappeared when heating in H_2 at a temperature slightly above 200°C.



(a) Au-Cu dimer under 2% O_2 in Ar during heating from 50 to 250°C followed by cooling. The blue line is the first temperature ramp and the red- the second. Between each ramp the samples where reduced by placing them in H_2 during a temperature ramp.



(b) Au-Cu dimer under 4% H_2 in Ar during heating from 50 to 300°C followed by cooling. The red line corresponds to the first temperature ramp and the red- the second. Between the two ramps the structures were placed under O_2 to become fully or partially oxidized.

Figure 6.7: Peak position difference between the two polarizations peak position during temperature ramps. The two colors represent separate temperature ramps, solid lines show the changes during heating and dotted lines show the changes while cooling.

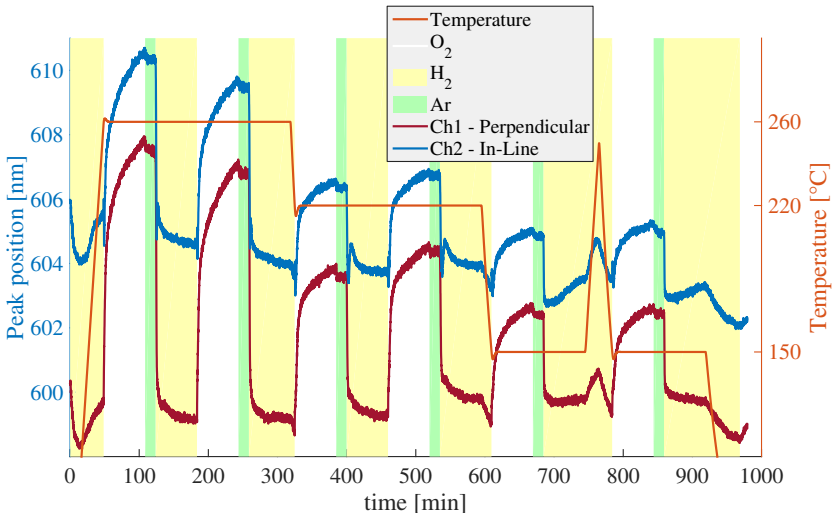
6.2.2.2 *Cycles*

The measurements made with polarized light were carried out with the same flow-rate and concentration of gases as the measurements described in section 6.2.1. Every cycle consists of 1h in O_2 followed by 15 minutes in pure Ar, then the gases are changed to H_2 for another hour.

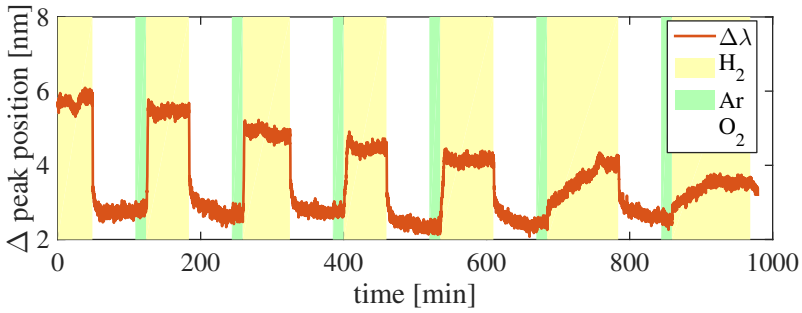
Figure 6.8 shows the response of the peak position of the two polarization dependent extinction spectra. The same trend as for unpolarized light is seen for both channels with a blue-shift on introduction of O_2 and red-shift when H_2 is introduced. When switching from 2% O_2 in Ar to pure Ar in the end of each O_2 period a small but clear blue-shift is seen for both channels.

The difference between the two polarization directions is presented in 6.8b. Here the perpendicular polarization is used as a adjustable baseline to take care of reactions not related to the changes in the Cu nanoparticle. It can be seen that there is a clear reversible change in the difference between the channels corresponding to the exposure of H_2 or O_2. The difference between the channels can be seen to decrease on exposure to O_2 and increase to the original peak separateion when H_2 is introduced.

To easier visualize the effects of the different cycles the oxidation and reduction steps are separated and explained separately.



(a) Response to the separate polarization directions. Ch1 corresponds to the perpendicular direction and Ch2 is in-line (parallel) with the two nanostructures.



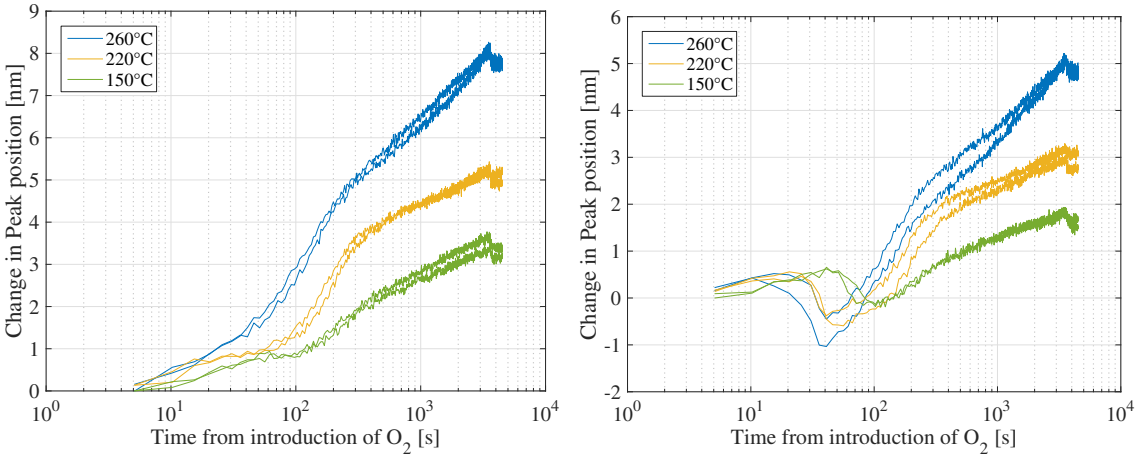
(b) Difference in peak position between the two polarizations. $\Delta\lambda = Ch2 - Ch1$ from the figure above.

Figure 6.8: Peak position response when Au-Cu structure is exposed to alternating H_2–O_2 cycles indicated by colors, at different temperatures. The first two cycles are at 260°C, the middle two at 220°C and the last two at 150°C. The spike seen in both channels at just before 800 minutes is due to heating of the sample to ensure the reduction happened.

Response to O_2 The response to 2% O_2 in Ar at different temperatures is presented in fig. 6.9 for the two measured polarization directions. Here both signals show a tendency to be moving against longer wavelengths over time. This is the same behavior seen for the measurements made with unpolarized light. The big difference between the two polarized signals is seen between 10–50 s where the spectrum taken in-line (6.9b) of the two structures shows a quite large blue-shift compared to the channel polarized perpendicular to the structures (6.9a). By comparing the different temperatures, the blue-shift seems to be quicker and larger at higher temperatures. To isolate the changes induced by changes in the Cu-particle, data of the perpendicular polarization was subtracted from data of the measurement made in-line. This shows the difference between the two peak positions over time and shows how the two peaks move relative to each other. The resulting change of the peak position difference of the two signals during oxidation is presented in fig. 6.9c. The difference between the two signals seems to be almost constant at all times, except in the region 10 – 40 s where the blue-shift was seen in fig. 6.9b for the channel polarized in line with the two structures. This change of the relative position of the two channels is proposed to correspond to the oxidation of copper nanoparticle into copper oxide.
After 1h in O_2 the flow was changed to pure Ar. This can be seen as a small (0.2 nm) blueshift in both signals at the end of the measurement. After this the signal remained constant without continuing the drift towards longer wavelengths. This indicates that the drift seen in the end of each measurement is a result of the O_2 present.

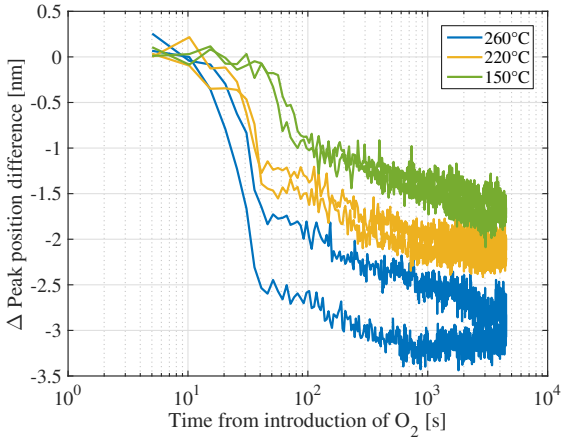
The change of substrate material from borosilicate glass to fused silica with a layer of silicon nitride on top changed the plasmonic response in the beginning of the measurement. A comparison of the response to O_2 using borosilicate glass presented in fig. 6.4b to the response when using silicon nitride coated glass in fig. 6.9 is presented in fig. 6.10. The values presented in fig. 6.10 have been normalized so the maximum peak change for all measurements is 1. In the silicon nitride case the response of both polarization directions is presented because the un-polarized measurement made on the borosilicate sample is presumed to be a weighted average of the two polarization directions. The biggest difference due to the change of substrate material can be seen during the first 20 s. The borosilicate measurement has a quick red-shift during these first seconds but the latter does not show this kind of behavior.

Response to H_2 In fig. 6.11 the response of the plasmonic peak position when 4% H_2 was introduced is presented. After about 30 s without any change in the plasmonic peak position a large blue-shift is seen for both channels. This is the inverse of what happens when the structures were exposed to O_2. The in-line polarized channel, presented in fig. 6.11b, has a red-shift after about 100 s for the measurements made at the two higher temperatures (220°C and 260°C). Because the parallel polarization is expected to show a larger change due to changes in the Cu, the red-shift seen at 100 s is proposed to be due to the reduction of Cu. More evidence that strengthens this statement is the fact that copper oxide is not expected to reduce at temperatures as low as 150°C and there is no shift at that temperature. To single out the changes in the Cu particle and avoid looking at substrate effects and reactions taking place on the Au, the difference between the peak position of the two channels is presented in fig. 6.11c. Here it can be seen that for the two higher



(a) Perpendicular polarization

(b) In-line polarization



(c) Difference between the two polarization measurements. Data from **(b) - (a)**.

Figure 6.9: Response of plasmonic peak position when 2% O_2 is introduced at different temperatures.

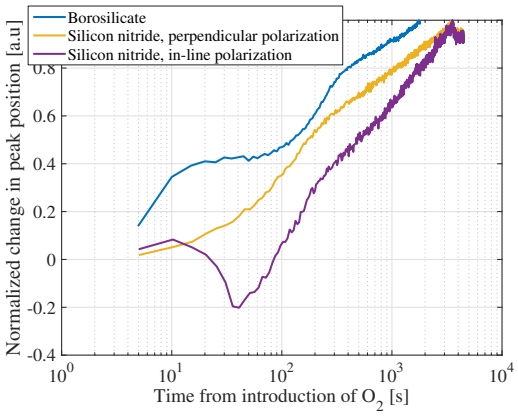
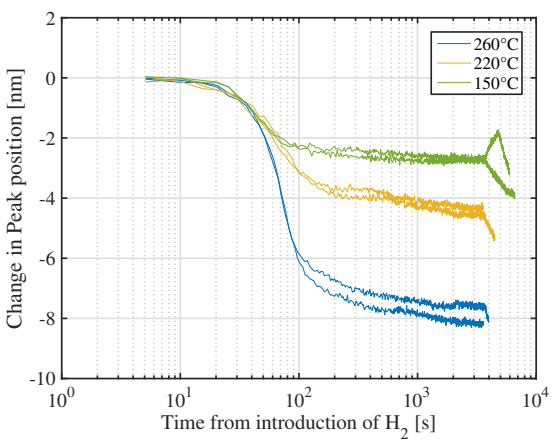
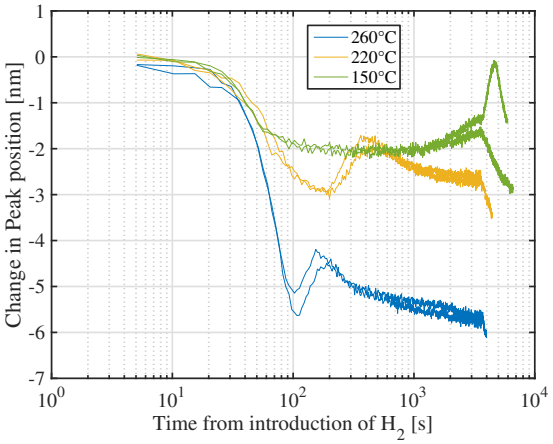


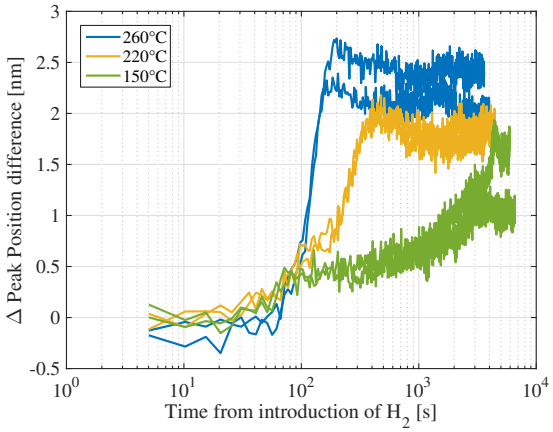
Figure 6.10: Dependence of the substrate material on the response of the plasmonic peak when introducing O_2 to similar Au-Cu structures. The borosilicate glass was measured at 280°C and the silicon nitride at 260°C. The biggest difference can be seen during the first 20 s where a red-shift is seen for the borosilicate substrate but not for the silicon nitride.



(a) Perpendicular polarization



(b) In-line polarization



(c) Difference in peak position between the two polarization directions.

Figure 6.11: Response of the plasmonic peak position of Au-Cu structure when exposed to H_2 at three different temperatures.

temperatures the difference between the two peak positions is almost constant before and after the increase of the difference starting at 100–200s. For the lowest temperature (150°C) there is a slow red-shift that goes on for 1h. For one of the measurements at 150°C the temperature was increased during the last minutes of the measurement. This can be seen at the end of one of the 150°C curves where a quite sharp increase in the peak position of the two measurements is seen. In agreement with what is expected, the reaction happens at earlier times and completes faster at higher temperatures. The shift is also bigger for the higher temperature, which was also seen for the oxidation reactions.

6.2.3 Effects of redox cycles on the structures

When oxidizing and reducing metals there is a risk that structural changes will occur. Incorporating O_2 into the material changes the crystalline structure of the material and forces the atoms to change positions. The high temperatures used for reactions also make it possible for atoms in the structure to become mobile and move around. To investigate the

effects of repeated cycles of H_2 and O_2 the samples were imaged after a number of cycles in SEM. In fig. 6.12 a few dimer structures are imaged. The Cu particles can be seen to have moved around and some even appear to have disintegrated into smaller particles. For reference the same kind of structures before exposure to cycles are presented in fig. 5.6a. These structural changes will most certainly affect the corrsponding measurements and have to be taken into account. Because ensemble measurements are made on several structures at the same time it is hard (or even impossible) to keep track of each of the individual particle geometries that contribute to the measurement. One way to eliminate this uncertainty is to do the same measurement on a single structure and at the same time keep track of the structural changes taking place in that specific structure.

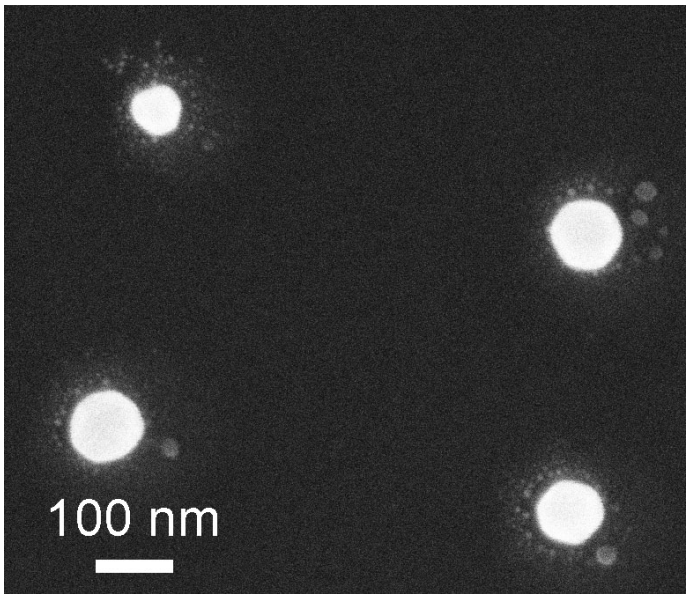


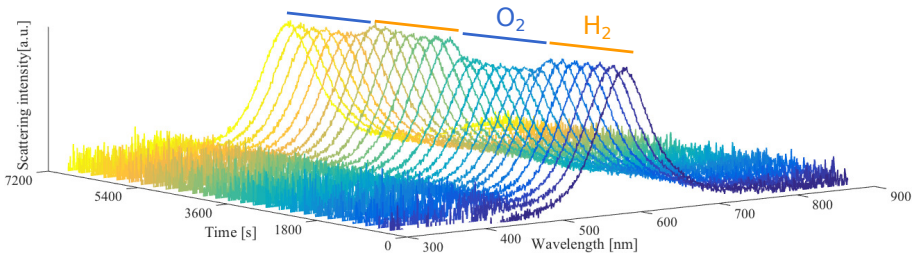
Figure 6.12: Au-Cu structures after being cycled in O_2 and H_2 at high temperature. The small Cu structure to the right of the larger Au-disk has moved, disappeared or disintegrated in some cases.

6.3 Single particle spectroscopy of Au-Cu Dimer

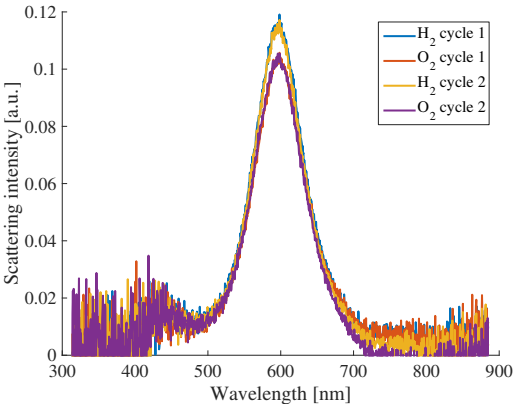
A single structure consisting of an Au disk with diameter 97nm and nominal thickness of 50 nm placed 5 nm from a Cu disk with a diameter of 29 nm and a nominal thickness of 20 nm was selected in a SEM and is presented in section 4.5. The structure was placed on a Si substrate covered by 50 nm thermally grown silicon oxide. The position of the structure on the substrate was mapped in the way shown in fig. 4.2. The scattering spectrum of the single structure was measured and the changes of it due to introduction of H_2 and O_2 at different temperatures was investigated.

6.3.1 Au-Cu structure at different temperatures

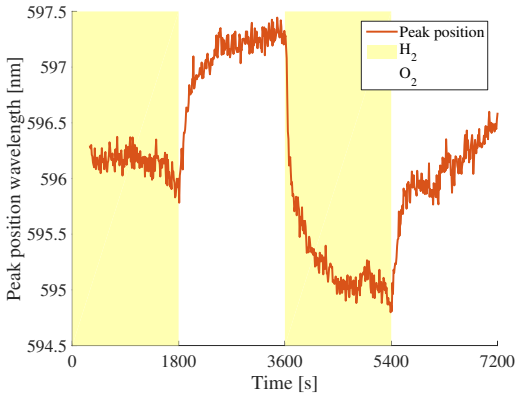
In fig. 6.13a the scattering spectrum of the single structure over time is presented. During this time the temperature was held at a constant level of 240°C, the gas flow was held at a constant flow-rate of 90 ml/min and the gas-composition was varied. From the beginning the structure was placed under a constant flow of 5% H_2 in Ar with flow-rate 90 ml/min. After 30 minutes the gas was changed to 2% O_2 in Ar, resulting in a decrease in the scattering intensity. After another 30 minutes the original H_2 flow was introduced resulting in an increase of the peak intensity, then O_2 was introduced again resulting in the same behavior as the first time.



(a) Change in scattering spectrum of a single Au-Cu structure when changing surrounding gas mixture. The temperature was held constant at 240°C.



(b) Scattering spectrum of Au-Cu structures under different surrounding gas composition. Note the reversibility.



(c) Peak position variation over time.

Figure 6.13: Plasmonic response of a Au-Cu dimer at 240°C in 2% O_2 and 5% H_2 in Ar.

In 6.13c the peak position change is presented showing a red-shift when introducing O_2 and a blue-shift when introducing H_2. To illustrate the reversible behavior of the scattering spectrum four overlaid spectra during the cycles are presented in 6.13b.

The same measurement was repeated for several temperatures and the resulting change of the peak wavelength is presented in fig. 6.14. Similar to the measurements made on ensembles of the same kind of structures, introduction of O_2 results in a red-shift and introduction of H_2 results in a blue-shift. In O_2 there is first a large jump of the peak

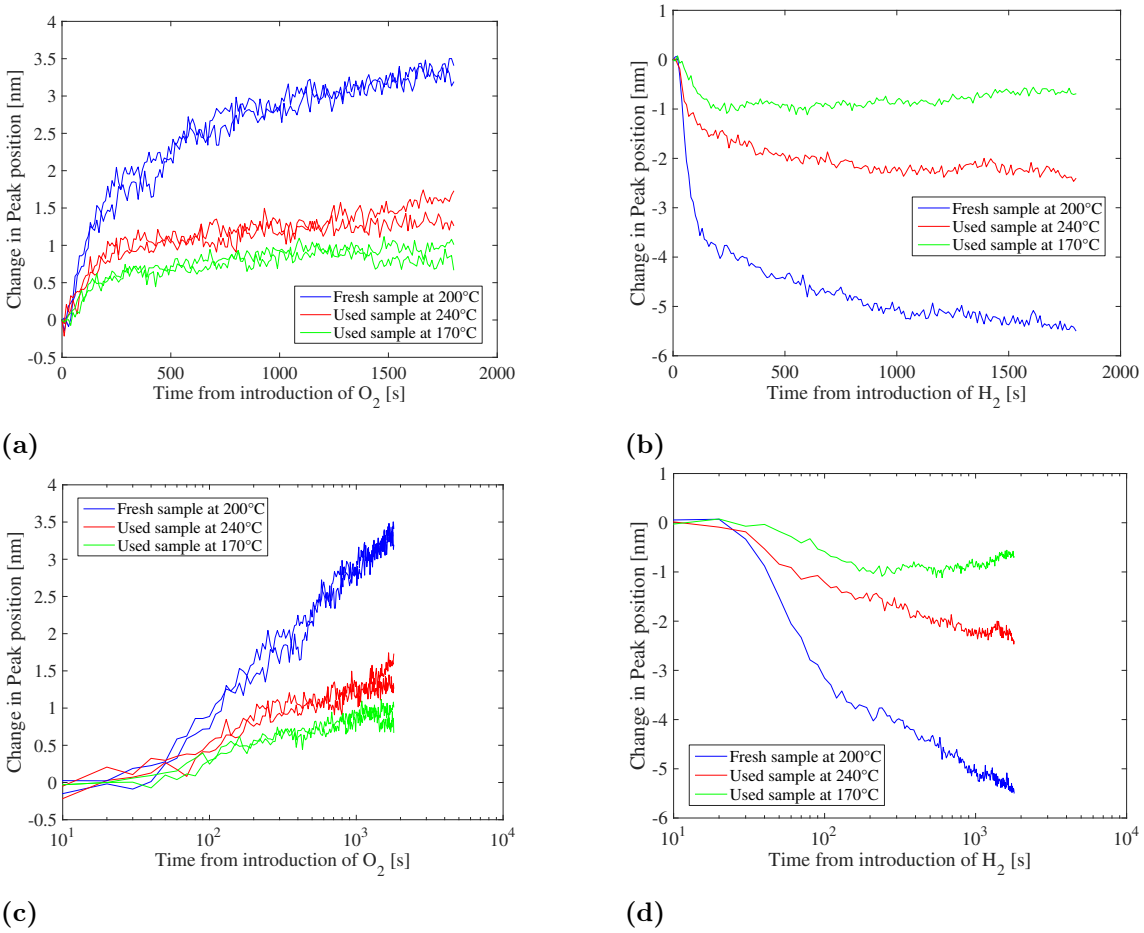


Figure 6.14: Peak position response when introducing O_2 or H_2 at different temperatures. Repeated lines during oxidation represent separate experiments.

position followed by a slower transition against longer wavelengths. In the logarithmic time-scale of the oxidation, presented in fig. 6.14c, the change in peak position starts after 50 s and appears to be linear for the full 30 minutes.

The largest peak shift is seen at 200°C followed by the measurement at 240°C and the smallest shift is seen for the lowest temperature of 170°C. This is not in correlation with what was seen for ensemble measurements of the same kind of structures. The reason for this is proposed to be due to degradation of the particle that was investigated. The measurement that was made first was the one at 200°C and it has therefore been labeled "fresh" to indicate that it was a new structure used for those measurements. When imaging the chosen structure in SEM after several cycles in H_2 and O_2 the structure had changed in a way presented in fig. 6.15. The Cu placed to the left of the large Au disk has seemingly disappeared which could lead to a significant decrease in the signal change when changing the gases.

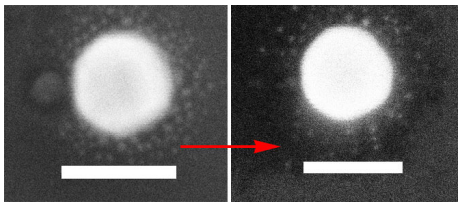


Figure 6.15: Change of the chosen Au-Cu structure after several cycles of H_2 and O_2 in different temperatures. The Cu to the left of the large Au disk has disappeared. The scale bars represent 100 nm.

6.3.2 Reference measurements on single Au disk

To make sure the signal observed in the Au-Cu structure came from oxidation and reduction of the Cu a reference measurement of a single Au disk was performed. The response of the plasmonic peak position of a single Au disk when exposed to a constant gas flow of 90 ml/min consisting of either 2% O_2 in Ar or 5% H_2 in Ar is presented in fig. 6.16.

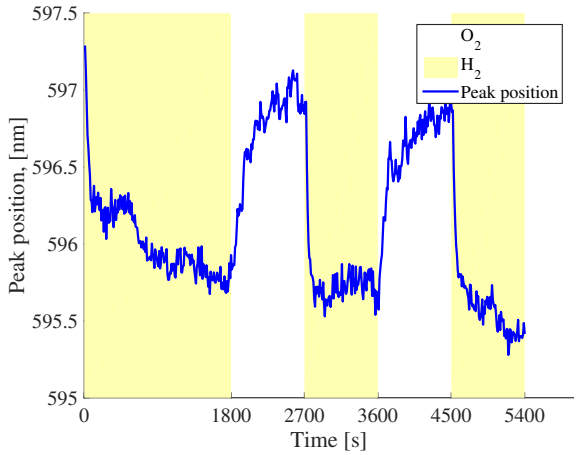
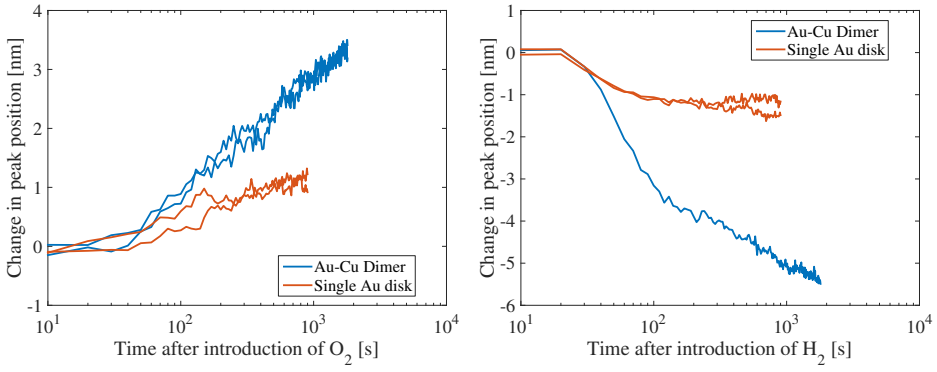


Figure 6.16: Plasmonic peak position of single Au disk under alternating 5% H_2 and 2% O_2 in Ar. The temperature was held constant at 200°C.

In fig. 6.17 the peak position response of the single Au disk is presented together with the response of the Au-Cu dimer discussed in the previous section. It can be seen that even a single Au put under reducing or oxidizing atmosphere had a response in its optical signal. At the introduction of O_2 to the structure the spectrum slowly started to move against longer wavelengths and when introducing 5% H_2 the peak returned to its initial state after a few minutes.
Compared to the Au-Cu structure the single Au did not have the large jump in peak position seen in the dimer and the speed of the reaction seemed to be slower.
The proposed reason for the change in peak position of the single Au structure is due to reactions taking place on the substrate and due to adsorbed species on the Au surface. Previous experiments, using Time-resolved in situ diffuse reflection infrared Fourier transform (DRIFT), has shown that SiO_2 substrates with Pt nanoparticles adsorb H_2[40]. The role of the nanoparticle is to act as a site where H_2 molecules are dissociated and then spill over to the substrate. Au hemispheres have also been shown to change their plasmonic spectra



(a) Under 2% O_2 **(b)** Under 5% H_2

Figure 6.17: Plasmonic peak position change of Au-Cu Dimer and single Au disk when exposed to different gas compositions. Both structures where placed on SiO_2-substrates and the temperature was held at 200°C. Repeated lines are separate experiments.

when exposed to H_2 due to formation of metastable AuH_x[39].
The Au disk in the experiment made in this thesis is therefore proposed to act in a similar way and the changes of the substrate induce a measurable change in the plasmonic peak of the Au disk.
Another possibility that has been considered is that of a photocatalytic effect taking place around the plasmonically active structures. Dissociation of H_2 on Au nanoparticles due to photocatalysis has recently been shown[43]. However it was concluded by Linic et.al. that the light intensities required to reach a measurable catalytic effect were significantly higher than the ones used for the measurements made here. A simple way of ruling out light affected reactions would be to block out the light for a time and then continue the measurement and see if the spectral shifts continued without the light present.
It is hard to determine which parts of the peak change seen in the dimer that correspond to changes taking place in the Cu, and which correspond to changes in the substrate and/or the Au particle itself. This problem was partially handled in the ensemble case by switching to an alternative substrate material and the same thing could be implemented for single particle measurements. By constructing a system that allows for polarization dependent measurements of single particles the effects connected to reactions taking place in the Cu could also be captured.

7

Conclusions

SHCL was used to fabricate structures consisting of Au acting as a sensor and a second material acting as reactive centre. The size and placement of nanosized structures could be finely tuned to enable fabrication of complex structures for different applications. The structures fabricated could be made with a large surface coverage to enable plasmonic sensing of an ensemble and low coverage – allowing measurements of single structures, both fabricated at identical conditions.
Au trimer structures, built as self-similar antennas, with a 15 nm Pd disk placed in the hottest spot were fabricated and a hydride formation experiment was performed to confirm that the fabricated structure worked as proposed.

Structures consisting of a Au disk with a smaller Cu disk were fabricated to investigate the plasmonic response of this structure when oxidizing and reducing the Cu. These measurements showed that changes in the Cu could be detected by measuring how the plasmonic peak of the sample changed over time when exposed to different gases. Further, the use of polarized light showed that it is possible to single out effects taking place in a specific structure placed besides a larger plasmonic antenna. This makes it possible to make drift corrected measurements by using a certain polarization of light as a baseline measurement. The method shows promise as an in-situ method of measuring oxidative states of nano-sized structures.

Single particle spectroscopy Single particle spectroscopy of small Cu particles has been shown to be possible. A structure consisting of a small Cu close to a larger Au antenna showed a large change in it's scattering spectrum when exposed to a oxidizing or reducing atmosphere.

7.1 Outlook

This work has mostly been to demonstrate the possibility of SHCL to make complex structures with a wider set of materials than shown before. Further investigation of how single structures of Au and Cu behave under oxidation and reduction have to be made to make sure the process is fully understood. As a next step, looking closer at the reaction kinetics of the structure would be of interest. To verify the composition of the structures after reactions, XPS measurements could be included. Theoretical models, based on for example FDTD, of the system would be of interest to see how the LSPR is expected to

behave when different layers of oxides are formed in the Cu particle. Simulations of that kind could also give information if it seems theoretically possible to distinguish between different oxides due to the resulting plasmonic spectra.
It would also be of interest to investigate the lower size limit of the Cu particle where indirect plasmonic sensing would still be possible. This limit could possibly be decreased by fabricating more complex antenna structures similar to the self-similar antenna used for detection of hydrogenation in Pd.
For single particle measurements an addition of polarized light could be a way to single out the effects taking place in the Cu in the same way as for the ensemble measurements. This would make it possible to detect changes related to reactions on the substrate. Single particle measurements also suffer from drift of the spectrum, both due to physical movement of the experimental setup and due to changes of the particle as the reactions undergo. The possibility to measure two polarizations of light simultaneously would make it possible to use the "off-particle" measurement as a baseline measurement that could be used to compensate for the drift.
The possibility to link the plasmonic peak behaviour of the Cu nanoparticles to kinetics of the redox reactions taking place in them would be a natural next step.
With the knowledge of how the optical properties of these sensors behave depending on the oxidative state of Cu application in catalytic sensing could be actualized. A future experiment could be to create nano-channels with the ability to measure the gas-flows in and out from a sample while at the same time measuring the plasmonic peak properties. With this a measure of the exact reactions occurring over one, or several, catalytic nanoparticle(s) could be indexed while knowing which oxidative state the catalytic particle had during the reaction. This could give interesting insight to how catalytic reactions work.

Acknowledgements

To start I would like to thank Christoph Langhammer for making it possible for me to do this thesis and for all the help moving the project forward. I also want to thank Svetlana Syrenova for introducing me to the cleanroom and teaching me basically all fabrication- and characterization methods used in this thesis.
David Johansson, thanks for great discussions and for letting me disturb you at any time, even when time was short.
A big thanks to Carl Wadell and Ferry Nugroho for helping me with the different reactor setups and to Joachim Frische for the input on single particle spectroscopy.
Thanks to the whole Chemical Physics group for nice lunches and fika during the past semester.
Finally, thanks to all my friends and family for all the help and support you have given me throughout the years!

David Albinsson, Gothenburg, August, 2015

Bibliography

1. Leonhardt, U. Optical metamaterials: Invisibility cup. *Nat Photon* **1,** 207–208 (Apr. 2007) (see p. 1).
2. Anker, J. N., Hall, W. P., Lyandres, O., Shah, N. C., Zhao, J. & Van Duyne, R. P. Biosensing with plasmonic nanosensors. *Nat Mater* **7,** 442–453 (June 2008) (see pp. 2, 10).
3. Langhammer, C., Zorić, I., Kasemo, B. & Clemens, B. M. Hydrogen Storage in Pd Nanodisks Characterized with a Novel Nanoplasmonic Sensing Scheme. *Nano Letters* **7.** PMID: 17850168, 3122–3127 (2007) (see pp. 2, 13, 40).
4. Liu, N., Tang, M. L., Hentschel, M., Giessen, H. & Alivisatos, A. P. Nanoantenna-enhanced gas sensing in a single tailored nanofocus. *Nat Mater* **10,** 631–636 (Aug. 2011) (see pp. 2, 9, 11–13).
5. Wadell, C., Syrenova, S. & Langhammer, C. Plasmonic Hydrogen Sensing with Nanostructured Metal Hydrides. *ACS Nano* **8.** PMID: 25427244, 11925–11940 (2014) (see pp. 2, 9, 10, 13, 40).
6. Atwater, H. A. & Polman, A. Plasmonics for improved photovoltaic devices. *Nat Mater* **9,** 205–213 (Mar. 2010) (see p. 2).
7. Giannini, V., Fernández-Dominguez, A. I., Heck, S. C. & Maier, S. A. Plasmonic Nanoantennas: Fundamentals and Their Use in Controlling the Radiative Properties of Nanoemitters. *Chemical Reviews* **111.** PMID: 21434605, 3888–3912 (2011) (see pp. 2, 11, 12).
8. McFarland, A. D. & Van Duyne, R. P. Single Silver Nanoparticles as Real-Time Optical Sensors with Zeptomole Sensitivity. *Nano Letters* **3,** 1057–1062 (2003) (see pp. 2, 9).
9. Syrenova, S. *Nanoplasmonic Spectroscopy of Single Nanoparticles Tracking Size and Shape Effects in Pd Hydride Formation* 64 (Institutionen för teknisk fysik, Kemisk fysik, Chalmers tekniska högskola, 2014) (see pp. 2, 9, 13, 32).
10. Li, K., Stockman, M. I. & Bergman, D. J. Self-Similar Chain of Metal Nanospheres as an Efficient Nanolens. *Physical Review Letters* **91.** doi:10.1103/PhysRevLett.91.227402 (2003) (see pp. 2, 12, 31).
11. Bohren, C. & Huffman, D. *Absorption and Scattering of Light by Small Particles* (Wiley, 2008) (see pp. 5–7).
12. Kreibig, U. & Vollmer, M. *Optical properties of metal clusters* (Springer Berlin, 1995) (see pp. 5, 7).

13. Ghosh, S. K. & Pal, T. Interparticle Coupling Effect on the Surface Plasmon Resonance of Gold Nanoparticles: From Theory to Applications. *Chemical Reviews* **107.** PMID: 17999554, 4797–4862 (2007) (see p. 8).

14. Kildishev, A. V., Borneman, J. D., Chen, K.-P. & Drachev, V. P. Numerical Modeling of Plasmonic Nanoantennas with Realistic 3D Roughness and Distortion. *Sensors* **11,** 7178–7187 (2011) (see p. 8).

15. Shegai, T. & Langhammer, C. Hydride Formation in Single Palladium and Magnesium Nanoparticles Studied By Nanoplasmonic Dark-Field Scattering Spectroscopy. *Advanced Materials* **23,** 4409–4414 (2011) (see pp. 9, 13).

16. Esteban, R., Borisov, A. G., Nordlander, P. & Aizpurua, J. Bridging quantum and classical plasmonics with a quantum-corrected model. *Nat Commun* **3,** 825 (May 8, 2012) (see p. 9).

17. Barbry, M., Koval, P., Marchesin, F., Esteban, R., Borisov, A. G., Aizpurua, J. & Sánchez-Portal, D. Atomistic near-field nanoplasmonics: reaching atomic-scale resolution in nanooptics. *Nano Letters,* null (2015) (see p. 9).

18. Chan, G. H., Zhao, J., Hicks, E. M., Schatz, G. C. & Van Duyne, R. P. Plasmonic Properties of Copper Nanoparticles Fabricated by Nanosphere Lithography. *Nano Letters* **7,** 1947–1952 (2007) (see pp. 10, 14).

19. Li, M., Cushing, S. K. & Wu, N. Plasmon-enhanced optical sensors: a review. *Analyst* **140,** 386–406 (2 2015) (see p. 10).

20. Langhammer", C. Size-Dependent Kinetics of Hydriding and Dehydriding of Pd Nanoparticles. *Physical Review Letters* **104.** doi:10.1103/PhysRevLett.104.135502 (2010) (see pp. 10, 13).

21. Toroghi, S. Photothermal response enhancement in heterogeneous plasmon-resonant nanoparticle trimers. *Physical Review B* **90.** doi:10.1103/PhysRevB.90.205414 (2014) (see p. 11).

22. Höppener, C., Lapin, Z. J., Bharadwaj, P. & Novotny, L. Self-Similar Gold-Nanoparticle Antennas for a Cascaded Enhancement of the Optical Field. *Physical Review Letters* **109.** doi:10.1103/PhysRevLett.109.017402 (2012) (see pp. 11, 12).

23. Syrenova, S., Wadell, C. & Langhammer, C. Shrinking-Hole Colloidal Lithography: Self-Aligned Nanofabrication of Complex Plasmonic Nanoantennas. *Nano Letters* **14.** PMID: 24697350, 2655–2663 (2014) (see pp. 11, 13, 22, 39).

24. Rechberger, W., Hohenau, A., Leitner, A., Krenn, J., Lamprecht, B. & Aussenegg, F. Optical properties of two interacting gold nanoparticles. *Optics Communications* **220,** 137–141 (2003) (see p. 12).

25. Halas, N. J., Lal, S., Chang, W.-S., Link, S. & Nordlander, P. Plasmons in Strongly Coupled Metallic Nanostructures. *Chemical Reviews* **111.** PMID: 21542636, 3913–3961 (2011) (see p. 12).

26. Pakizeh, T., Langhammer, C., Zorić, I., Apell, P. & Käll, M. Intrinsic Fano Interference of Localized Plasmons in Pd Nanoparticles. *Nano Letters* **9.** PMID: 19175307, 882–886 (2009) (see p. 13).

27. Vargas, W., Rojas, I., Azofeifa, D. & Clark, N. Optical and electrical properties of hydrided palladium thin films studied by an inversion approach from transmittance measurements. *Thin Solid Films* **496,** 189–196 (2006) (see p. 13).

28. Vukojević, S., Trapp, O., Grunwaldt, J.-D., Kiener, C. & Schüth, F. Quasi-Homogeneous Methanol Synthesis Over Highly Active Copper Nanoparticles. *Angewandte Chemie International Edition* **44,** 7978–7981 (2005) (see p. 14).

29. Schimpf, S., Rittermeier, A., Zhang, X., Li, Z.-A., Spasova, M., van den Berg, M. W. E., Farle, M., Wang, Y., Fischer, R. A. & Muhler, M. Stearate-Based Cu Colloids in Methanol Synthesis: Structural Changes Driven by Strong Metal–Support Interactions. *ChemCatChem* **2,** 214–222 (2010) (see p. 14).

30. Park, J. B., Graciani, J., Evans, J., Stacchiola, D., Senanayake, S. D., Barrio, L., Liu, P., Sanz, J. F., Hrbek, J. & Rodriguez, J. Gold, Copper, and Platinum Nanoparticles Dispersed on CeOx/TiO2(110) Surfaces: High Water-Gas Shift Activity and the Nature of the Mixed-Metal Oxide at the Nanometer Level. *Journal of the American Chemical Society* **132,** 356–363 (Jan. 2010) (see p. 14).

31. Yabuki, A. & Tanaka, S. Oxidation behavior of copper nanoparticles at low temperature. *Materials Research Bulletin* **46,** 2323–2327 (2011) (see pp. 14, 15, 41, 42).

32. Fredriksson, H., Alaverdyan, Y., Dmitriev, A., Langhammer, C., Sutherland, D., Zach, M. & Kasemo, B. Hole-Mask Colloidal Lithography. *Advanced Materials* **19,** 4297–4302 (2007) (see p. 18).

33. Franssila, S. in *Introduction to Microfabrication* 47–67 (John Wiley & Sons, Ltd, 2010). doi:10.1002/9781119990413.ch5 (see p. 19).

34. Wadell, C. & Langhammer, C. Drift-corrected nanoplasmonic hydrogen sensing by polarization. *Nanoscale* **7,** 10963–10969 (25 2015) (see pp. 26, 39, 40, 44).

35. Schneider, C. A., Rasband, W. S. & Eliceiri, K. W. NIH Image to ImageJ: 25 years of image analysis. *Nature methods* **9,** 671–675 (2012) (see p. 31).

36. Thornton, J. A. & Hoffman, D. Stress-related effects in thin films. *Thin Solid Films* **171,** 5–31 (1989) (see p. 33).

37. Lee, F. Y., Fung, K. H., Tang, T. L., Tam, W. Y. & Chan, C. Fabrication of gold nano-particle arrays using two-dimensional templates from holographic lithography. *Current Applied Physics* **9,** 820–825 (2009) (see p. 36).

38. Rodriguez, J., Kim, J., Hanson, J., Perez, M. & Frenkel, A. Reduction of CuO in H2: In Situ Time-Resolved XRD Studies. English. *Catalysis Letters* **85,** 247–254 (2003) (see p. 41).

39. Sil, D., Gilroy, K. D., Niaux, A., Boulesbaa, A., Neretina, S. & Borguet, E. Seeing Is Believing: Hot Electron Based Gold Nanoplasmonic Optical Hydrogen Sensor. *ACS Nano* **8,** 7755–7762 (Aug. 2014) (see pp. 43, 55).

40. Wallin, M., Grönbeck, H., Spetz, A. L., Eriksson, M. & Skoglundh, M. Vibrational Analysis of H2 and D2 Adsorption on Pt/SiO2. *The Journal of Physical Chemistry B* **109.** PMID: 16852153, 9581–9588 (2005) (see pp. 43, 54).

41. Collins, S. S. E., Cittadini, M., Pecharromán, C., Martucci, A. & Mulvaney, P. Hydrogen Spillover between Single Gold Nanorods and Metal Oxide Supports: A Surface Plasmon Spectroscopy Study. *ACS Nano.* PMID: 26154166, null (see p. 43).

42. Johansson, D. *Localized surface plasmon nanoparticles for catalytic sensing* MA thesis (2015) (see pp. 44, 45).

43. Linic, S., Aslam, U., Boerigter, C. & Morabito, M. Photochemical transformations on plasmonic metal nanoparticles. *Nat Mater* **14,** 567–576 (June 2015) (see p. 55).